FRIEDRICH-SCHILLER-
UNIVERSITÄT
JENA

Charge State Tailoring for Relativistic Heavy Ion Beams

MASTER'S THESIS
submitted in fulfillment of the requirements
for the degree of Master of Science

written by
Felix Kröger
born in Luxembourg

Friedrich-Schiller-Universität Jena

2018

1st supervisor : Prof. Dr. Thomas Stöhlker

2nd supervisor : Dr. Günter Weber

Abstract

In this work charge state distributions of heavy ions have been calculated for the production of effective stripper foils for heavy ion acceleration facilities. In this context, the FAIR facility at GSI and the proposed Gamma Factory at CERN are presented, where the use of partially stripped, relativistic ions will be of special interest for upcoming experiments. To determine the charge state distribution as a function of penetration depth, various programmes have been applied, depending on the respective energy regime. For stripping scenarios in the lower energy regime, the GLOBAL code was applied, that allows to take into account up to twenty-eight projectile electrons for energies up to 2000 MeV/u. Since the GSI/FAIR facility can accelerate even low-charged uranium ions up to 2700 MeV/u, and the Gamma Factory at CERN considers a stripping scenario at 5900 MeV/u, another programme was needed. This is why for the stripping scenarios in the high energy regime, first the well-known CHARGE code was used. However, even though it can operate in the very high energy regime, it only takes into account bare, hydrogen- and heliumlike projectile charge states. To overcome this limitation, the recently developed BREIT code was verified and used for stripping scenarios in the high energy regime. As this code has no built-in treatment of the various charge-changing processes, it needs a multitude of information about the electron capture and loss cross sections as input parameters. Thus, for the calculation of charge state distributions with the BREIT code, cross sections were computed by well-tested theories and codes. The BREIT code together with the codes for the cross section computation were then applied for two studies: first for an exemplification study for the upcoming GSI/FAIR facility to show the practicability of the BREIT code together with the cross section programmes, and then for a study to find optimal stripper foils for the Gamma Factory study group at the CERN facility, in order to efficiently produce Pb^{80+} and Pb^{81+} ions from a Pb^{54+} beam before entering the LHC. Furthermore, experimental data of a beam time at ESR at GSI in 2016 was analysed, where a Xe^{54+} ion beam of several MeV/u was colliding with a hydrogen gas target. The data allowed the derivation of experimental NRC cross sections, and it was shown that the predictions of the EIKONAL code are in good agreement with these cross sections in an energy range most relevant for upcoming experiments at CRYRING@GSI.

Contents

1 Introduction

Upgrades of existing ion accelerators and also new facilities, like the facility for anti-proton and ion research FAIR[1] at GSI[2], are aiming to extend the range of achievable beam intensities and energies. A possible route to achieve most intense, relativistic ion beams effectively is to use lowly-charged, many-electron ions to reduce space-charge induced intensity limitations in the various ion acceleration and storage facilities. This implies that for experiments relying on well-defined, few-electron charge states, it is necessary to produce the required charge states with stripper foils optimized for the specific experimental parameters. However, corresponding data on the charge state distribution for the production of stripper targets for the stripping of heavy ions in the high relativistic energy regime is very rare. Therefore, a recently developed programme, called BREIT[3] code, will be adapted and verified, to see if it is suitable to fulfil this task. After that, studies will be presented, representing exemplifications of how this code can be used for future tasks at the acceleration facilities. To illustrate the necessity of such studies, in the following two of today's largest accelerator facilities are presented, where the use of fast, many-electron ions is foreseen: the aforementioned GSI/FAIR and the CERN[4] facilities. Each of them is capable of accelerating heavy ions to relativistic and ultra-relativistic energies. However there is an important difference between them both: while GSI/FAIR is designed to provide a broad spectrum of ion species and charge states, the main parts of the CERN facility are primarily optimized for the usage of protons and lead ions. In the following an example use-case for both of the mentioned facilities will be shown, each chosen in regard to the importance for the progress of this work: uranium for GSI and lead for CERN.
After the presentation of the facilities and the detailed function of stripper targets, the charge exchange processes will be explained, as well as the energy loss mechanisms. Subsequently, the calculation tools and computer codes used for charge state distribution studies in this work will be described. Then the results of the studies for the GSI/FAIR and CERN facilities will be discussed. At the end of this work an analysis of experimental data from a beam time at

[1] Facility for Anti-Proton and Ion Research
[2] Gesellschaft für Schwerionenforschung
[3] Balance rate equations of ion transportation
[4] Conseil Européen pour la Recherche Nucléaire

ESR[5] at GSI in 2016 will then be presented, that allows the determination of the total non-radiative electron capture (NRC) cross sections of bare xenon ions colliding with hydrogen atoms. The experiment is covering part of the energies available at the CRYRING@ESR[6], and is thereby allowing to verify the theory and code used for the calculation of the NRC cross sections for the future use at the mentioned facility for energies of a few MeV/u (depending on the projectile/target combination). This will be of special interest for experiments at CRYRING@GSI and therefore for potential future charge state distribution studies.

GSI

The GSI is a worldwide unique large-scale accelerator facility for heavy-ion beams, located in Darmstadt, Germany. Since it was founded in 1969, its research programme has continuously evolved and expanded with a focus on the physics of heavy ions. Nowadays, GSI covers experimental studies from atomic, nuclear, plasma and biophysics as well as from materials research. Moreover, at the GSI campus the international FAIR facility is currently under construction. The future beam lines path of this facility is including the heavy ion synchrotron SIS100[7], as well as various storage rings, and is represented by the red line in figure (1), whereas the beam lines path of the existing GSI facilities are denoted by the blue coloured line.

To produce an ion beam, lowly-charged ions are provided by ion sources of which several types exist that are optimized for certain charge states and materials. From an ion source, the ions are injected into the linear accelerator UNILAC[8], where they are accelerated and bunched using a radio-frequency high voltage. This linear accelerator, which was constructed as the first installation of the GSI facility, consists of two acceleration stages with a gas stripper in between. To produce a uranium ion beam, the first part accelerates lowly-charged uranium ions U^{4+} to 1.4 MeV/u, which allows the efficient production

[5]Experimentier-SpeicherRing

[6]This facility was originally named after the CRYogenic Stockholm ion source CRYSIS, for which it served as a subsequent synchrotron and storage RING. After it was transferred to GSI as a Swedish in-kind contribution to FAIR and installed subsequent to the ESR, it was renamed CRYRING@ESR.

[7]upcoming SchwerIonenSynchrotron with magnetic rigidity of 100 Tm

[8]UNIversal Linear ACcelerator

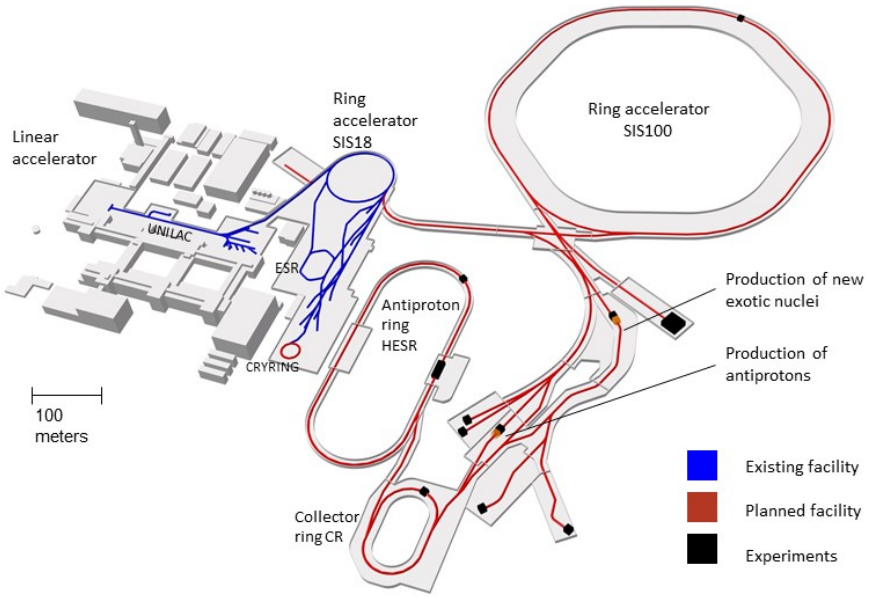

Fig. 1: Upcoming GSI/FAIR facility: the red lines mark the beam lines of the upcoming FAIR (Facility for Anti-proton and Ion Research) facility and the blue lines mark the beam lines of the present GSI facility. Taken from: [1]

of a U^{28+} beam after passing the gas stripper. The second acceleration stage then reaches up to 11.4 MeV/u, which enables the efficient production of U^{73+} using a stripper foil in the transfer beam line to the heavy ion synchrotron SIS18[9]. The SIS18 with its magnetic rigidity of 18 Tm is able to accelerate the ion beam to a maximum energy of roughly 1 GeV/u in the case of heavy elements [2, 3, 4, 5]. Injection into the experimental storage ring ESR, the main facility for atomic physics experiments at GSI, is done at a typical energy of 400 MeV/u if the aim is to store bare or hydrogen-like uranium. The last stripping stage is located in the transfer beam line from SIS18 to ESR. Experiments with stored ions in the ESR can be performed at the internal gas target and the electron cooler, moreover it is also possible to let the ions interact with a laser beam. The ESR can also be used as a deceleration stage to slow down highly charged ions and to transfer them to the HITRAP[10] facility and the recently installed CRYRING@ESR, which is the first installation of the future FAIR facility to be

[9] existing SchwerIonenSynchrotron with magnetic rigidity of 18 Tm
[10] Heavy Ion Trap

completed.

For the main part of FAIR that is currently under construction, SIS18 will be used as an injector into the new SIS100, from which high intensity ion beams will be delivered to several end stations and storage rings [6]. With a rigidity of 100 Tm, this synchrotron can accelerate ion beams into the highly relativistic energy regime, allowing to create heavy ion beams of mutliple GeV/u of energy. For the example of uranium, the 1.4 MeV/u U^{28+} ions in the UNILAC would skip the second stripping stage and would instead be accelerated and injected without further stripping into the SIS18. Afterwards it would be guided into the SIS100, where it can then be accelerated up to $\sim$ 2.7 GeV/u. After extraction from the SIS100, a specific charge state of interest can be produced, depending on the choice of the stripper target material and thickness. The prepared beam can then be used immediately, or be transferred in an ion storage ring, where it can be slowed down and then be guided to different experiments. For the atomic physics division (the atomic physics collaborations SPARC[11]) the APPA[12] cave and the high-energy storage ring HESR[13] are of special interest. The range of operating energies of the FAIR and GSI facilities is schematically depicted in figure 2, and in table 2 some beam parameters of the different facilities are listed. Fully or partially stripped heavy ion beams will be used in the APPA cave for fixed-target (single-pass) experiments at highly relativistic energies, or can be stored in the HESR. These experiments are mostly covered by the SPARC collaboration. Another task of the HESR will be the collision of protons with anti-protons within the scientific programme of

Table 1: Capabilities of the GSI/FAIR complex for uranium ions.

Facility	**Magnetic Rigidity**	**Projectile**	**Maximum Beam Energy**
UNILAC	-	U^{28+}	11.4 MeV/u
SIS18	max. 18 Tm	U^{28+}	200 MeV/u
SIS100	max. 100 Tm	U^{92+}	10.7 GeV/u
HESR	max. 50 Tm	U^{92+}	4.9 GeV/u
ESR	max. 10 Tm	U^{92+}	1 GeV/u
CRYRING@ESR	max. 1.4 Tm	U^{92+}	$\lesssim$ 300 keV/u to $\sim$ 14 MeV/u

[11] Stored Particles Atomic physics Research Collaboration
[12] Atomic, Plasma Physics and Applications
[13] High-Energy Storage Ring

the PANDA[14] collaboration. The SIS100 allows proton beams of 29 GeV, which is high enough to create anti-protons at an anti-proton separator target [7].

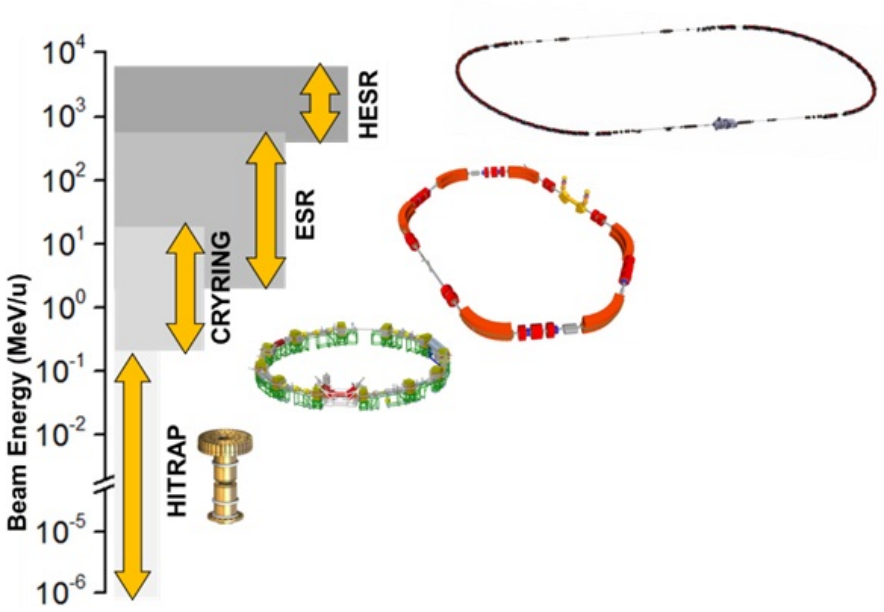

Fig. 2: Schematic overview of the GSI and FAIR facilities, covering kinetic energies of trapped and stored highly-charged ions from rest up to the highly relativistic energy regime. Taken from: [8]

CERN

CERN was founded in 1952 by 22 collaborating countries to establish a world-class fundamental physics research facility in Europe [9]. To gain knowledge of the most elementary particles known, high-energy physics research experiments are performed with large accelerators including the world's largest and most powerful accelerator, the LHC[15]. The LHC accelerator is the successor of the large electron-positron collider LEP[16] that was built in the early 1980s. The construction of the LHC was decided in 1994. By re-using the 27-km circumference tunnel of the LEP, after its final shutdown in 2000, the LHC made it possible to accelerate and collide hadrons and thus ions in the ultra-relativistic regime of several TeV/u [10].

[14] anti-Proton ANnihilations at DArmstadt
[15] Large Hadron Collider
[16] Large Electron-Positron collider

To produce ion beams at CERN, once again initially neutral atoms are supplied to an ion source, where low-charged ions are produced by heating a highly purified sample of gaseous materials, of vaporized solid, or of fluid materials. In case of Pb^{29+} this is done at 800°C. Then the ions are extracted to the LINAC 3[17] where they are bunched and accelerated, to 4.2 MeV/u for lead, and then stripped by passing a carbon foil, resulting for the lead ions in an intense beam of Pb^{54+}. This ion beam is then accelerated to higher energies at the LEIR[18], before it is guided into the PS[19]. The PS accelerates the ions delivered by the LEIR to relativistic energies, namely 5.9 GeV/u in case of lead ions, before they pass once again a stripper foil, where they can become fully stripped. Such ions are then sent into the even larger SPS[20] that allows to accelerate naked ions to even higher energies, like 177 GeV/u for Pb^{82+} [10]. Finally, this heavy ion beam is injected into the LHC, that accelerates heavy ions as the Pb^{82+} up to 2.76 TeV/u [11].

Table 2: Design parameters of the CERN complex for lead ions.

Facility	**Magnetic Rigidity**	**Projectile**	γ	**Max. Energy**	**Max. Proton Energy**
LEIR	4.8 Tm	Pb^{54+}	1.078	72.2 MeV/u	0.78 GeV
PS	86.67 Tm	Pb^{54+}	7.334	5.9 GeV/u	25.17 GeV
SPS	1504 Tm	Pb^{82+}	191.017	177 GeV/u	450 GeV
LHC	23352 Tm	Pb^{82+}	2963.982	2760 GeV/u	7000 GeV

A part of the recently (2016) set up 'Physics Beyond Colliders' study group is exploring possibilities to broaden the present CERN research programme, by using the infrastructure of the existing accelerators. Thus a multi-purpose Gamma Factory could be created, that pushes the intensity limits of presently operating light-sources by at least seven orders of magnitude, in the particular interesting domain of γ-ray energies of $1 \leqslant \hbar\omega \leqslant 400\,\mathrm{MeV}$. This domain is out of reach of FEL[21]-based light sources, opening new research opportunities at CERN [13]. For the proposed Gamma Factory it would be required to use light sources, producing laser photons which are absorbed by the electrons of partially stripped relativistic ions. With the proper energy adjustment of

[17] LINear ACcelerator
[18] Low Energy Ion Ring
[19] Proton Synchrotron
[20] Super Proton Synchrotron
[21] Free-Electron Laser

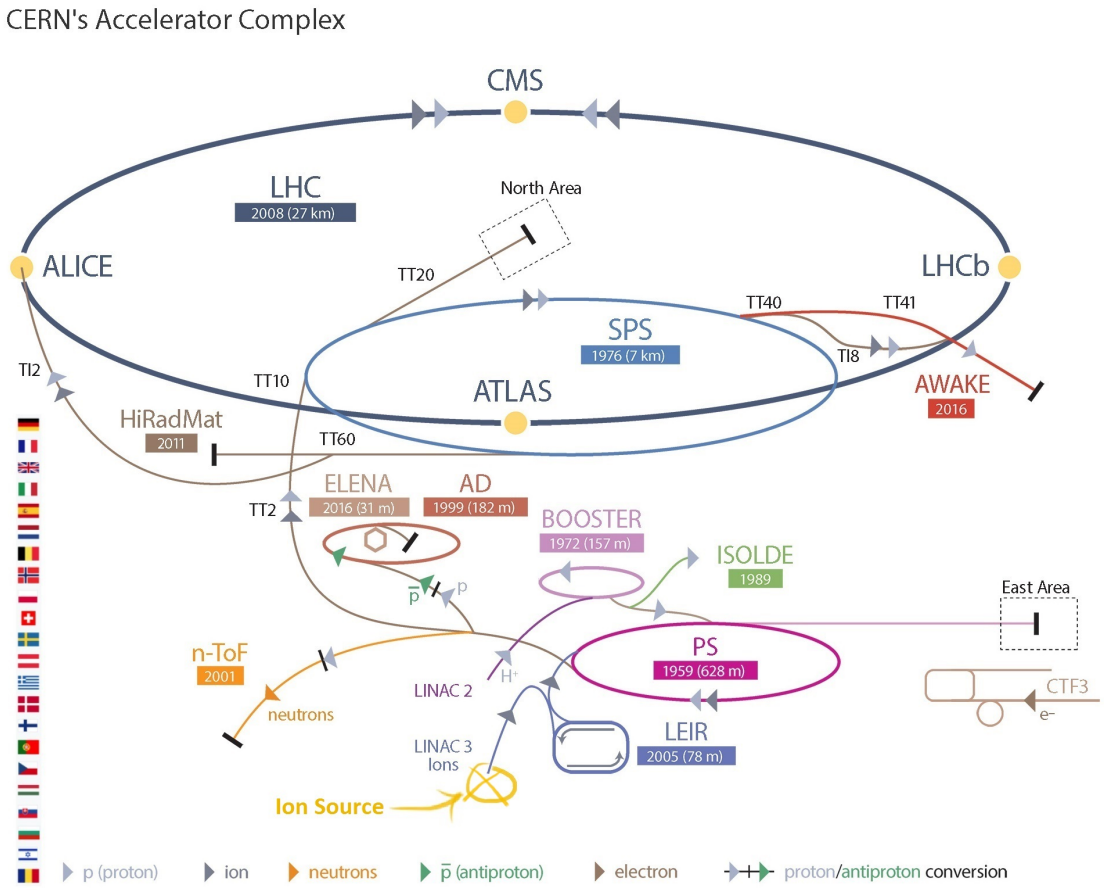

Fig. 3: CERN facilities: LHC is shown in dark blue and SPS in bright blue. The direction of ions through the accelerators is shown in dark grey. Taken from: [12]

the ion beam, these electrons are then excited resonantly into higher energetic states of the ions. The process where an excited electron then falls back into the ground state, is accompanied by re-emission of a photon. Due to the relativistic movement of the ions, this usually isotropic emission process becomes more favoured into the forward direction of the ion. During the absorption process, in the projectile's framework the movement towards the laser photons causes a Doppler blueshift. The same holds for the photon emission in the laboratory framework, where high energy gamma rays are emitted. The idea is to profit from these Doppler effects, using the ion beam as a high energy boost for the production of intense gamma rays, which can then be used for experiments. For this application, in this work stripper foils will be studied that could allow the production of hydrogen- or helium-like lead ($^{207}_{82}$Pb) projectiles that could

fulfil this task. These foils could be positioned either before the PS accelerator, where Pb^{54+} ions could be stripped at 72.2 MeV/u, or before entering the SPS, where ions could be stripped at 5900 MeV/u. The results will be presented and discussed in chapter 4 of this work.

After these detailed presentations of the accelerator facilities it is worth discussing some details of stripper targets.

Stripper Targets

To accelerate particles to high energies it is important that the projectiles are highly charged, so they can be efficiently affected by the applied electromagnetic fields. To achieve this requirement it is necessary to remove electrons from atoms in order to meet the specifications of the accelerator (for example magnetic rigidity, etc.). This task is performed by the stripper targets, being in gaseous or solid state phase. During the passage of an ion beam through such a target, projectile electrons are ionized in the collisions with target atoms. This leads to an increase in charge state until either the projectile ion leaves the target, or the equilibrium charge state is reached, where the cross sections for capture and for loss processes are in balance. At equilibrium the final charge state dis-

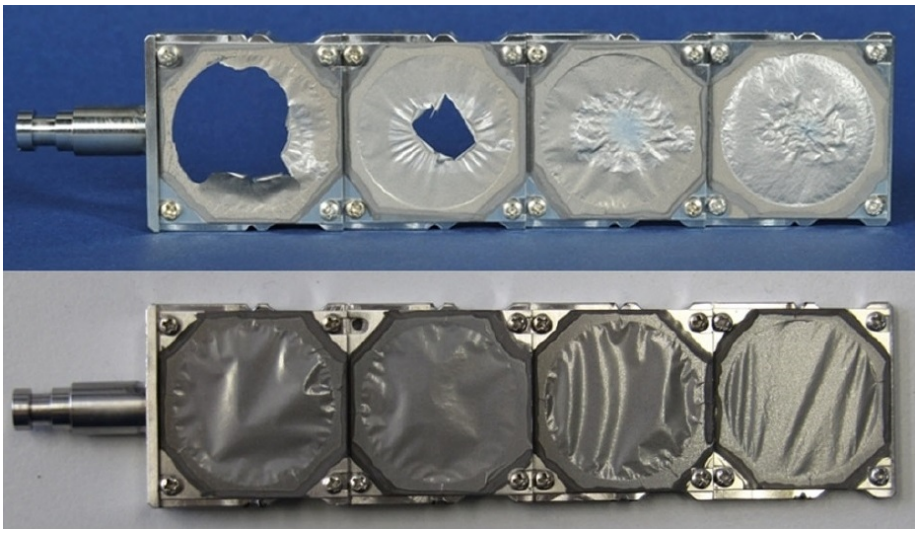

Fig. 4: Set of carbon stripper foils of different thickness before (bottom) and after (top) operation at the UNILAC at GSI with argon and uranium beams from a Penning ion source, as well as an uranium beam from a MEVVA ion source. Taken from: [14]

tribution is independent from the initial charge state of the ions. With regard to the upcoming high energy facilities, this work is focusing on the solid targets, since they operate much more efficiently in the high energy range, whereas low-density gas targets are preferably used for low-energy ions. The targets are used in the form of thin stripper foils that are fixed in a frame and placed into the beam-line. Some examples of such foils, before and after use, can be seen in figure 4.
As in most nuclear and particle physics experiments, which were the main drivers for the development of powerful accelerators, the presence of projectile electrons is not necessary or even undesirable, the main interest was usually to achieve the highest possible charge state for optimum acceleration. This is the reason why the main focus was given to produce fully stripped ions. However, many experiments in the realm of atomic physics require at least a few electrons in the initial state of the projectile and therefore with the upcoming FAIR facilities, it could be interesting to use partially stripped ions for new experiments. The choice of the ideal stripper foil is depending on many different aspects. Of course the yield of the charge state of interest has priority, but also the ability of the foil to sustain damage due to energy loss by the ion beam and its influence on the beam quality (i.e. energy and angular straggling) are relevant criteria.

2 Physical Basics of Ions Passing through Matter

Highly charged fast ions passing through matter are interacting with the atoms of the material mainly by charge-exchange processes and quasi-continuous energy loss. For heavy particles radiative energy loss (i.e. bremsstrahlung) is negligible and therefore the energy and angular straggling of an ion beam passing through matter can be attributed to elastic scattering from the target atom nuclei and inelastic collisions with the target electrons [15].
Due to the much larger radius of the electron orbit of the electron shell compared to the one of the nucleus, (having a diameter of 10^{-10} m, versus 10^{-13} m, respectively) nuclear interactions with the nuclei are relatively rare compared to the interactions with the electrons. Therefore, in the following only electronic interactions will be discussed.

2.1 Charge Exchange Processes

The description of the following charge exchange processes all rely on single electron approximations, i.e. the ionization or capture of an 'active' electron is treated without taking into account side-effects on the other electrons in the system, in particular multi-electron processes are neglected. However, the shielding of the positive nuclear charge Z, coming from the positively charged protons of the nucleus, by surrounding electrons can be taken into account by using an 'effective nuclear charge' Z_{eff}, with $Z_{P,eff} < Z_P$, as well as $Z_{T,eff} < Z_T$, as proposed for example by Slater [16]. This effective Z describes the respective charge seen by an electron near a nucleus, that is reduced by the coulomb force of other electrons in the same or lower atomic shells. To determine the charge state distribution of ion beams, the charge exchange is reduced in the calculations to single-electron loss and to radiative, as well as non-radiative single-electron capture. After each collision all deflection of the projectile ions from their initial path is neglected. In addition post-collision effects are not taken into account, like e.g. the Auger effect, which can lead to the loss of additional electrons once a deep-lying vacancy is created in the ion. Note that for the further proceeding of this work particle energy is referring to the kinetic energy of a particle.

2.1.1 Radiative Recombination (RR) and Radiative Electron Capture (REC)

There are two types of radiative capture processes of an electron. Radiative recombination (RR) describes the process where a free electron is captured into a bound state of an ion accompanied by photon emission. If instead the electron is initially bound to a target atom, the process is called radiative electron capture (REC). The energy of the emitted photon can be calculated with the following formula:

$$\hbar\omega = \mathrm{E_{kin,e}} - \mathrm{E_{b,e}} \quad , \tag{1}$$

with ω being the angular momentum of the photon, $\mathrm{E_{kin,e}}$ the kinetic energy of the captured electron, and $\mathrm{E_{b,e}}$ the binding energy of the captured electron into its bound state. The RR-process can be calculated very accurately by applying the principle of detailed balance on the existing results of its time-reversed process [17], the photoionization, that was already subject of theoretical studies since the beginning of quantum mechanics (see e.g. [18, 19, 20])[17, 21].

For the description of the REC process in high-energy collisions, where the electron has an initial binding energy in the target atom that is negligible compared to the kinetic energy in the projectile system, the impulse approximation can be applied [21]. In this approximation the loosely bound target electron is considered as quasi-free so that REC becomes identical to RR [17, 22, 23, 24]. The binding of the electron is now taken into account by folding the initial momentum distribution of the target electron, due to the movement of the projectile relative to the target atom, with the momentum distribution of the bound state of the target electron. The result is that an electron, initially moving with the kinetic energy $\mathrm{E_{kin,e}}$ in the projectile frame, is captured into a bound state $|\varepsilon_\mathrm{n}|$ of the projectile, accompanied by simultaneous emission of a photon of the following energy in the laboratory frame:

$$\hbar\omega = \frac{\mid \varepsilon_\mathrm{f} \mid -\gamma \mid \varepsilon_\mathrm{i} \mid +\mathrm{T_e} - \gamma \mathrm{v q_z}}{\gamma(1 - \beta cos\theta)} \quad . \tag{2}$$

In this formula ε_i and ε_f are the initial and final bound state, respectively, and $\mathrm{q_z}$ is describing the longitudinal momentum. $\mathrm{T_e} = (\gamma - 1)\mathrm{m_e c^2}$ is the kinetic energy of an electron, where $\mathrm{m_e}$ is denoting the mass of an electron, and c the speed of light. θ is the angle of the wave vector $\mathbf{k}$ with respect to the velocity direction, and $\gamma = (1 - \beta)^{-1/2}$ is denoting the Lorentz factor with the relativistic

factor $\beta = v/c$, where v is the projectile velocity [24]. The different processes are illustrated in the following figure (see figure 5).

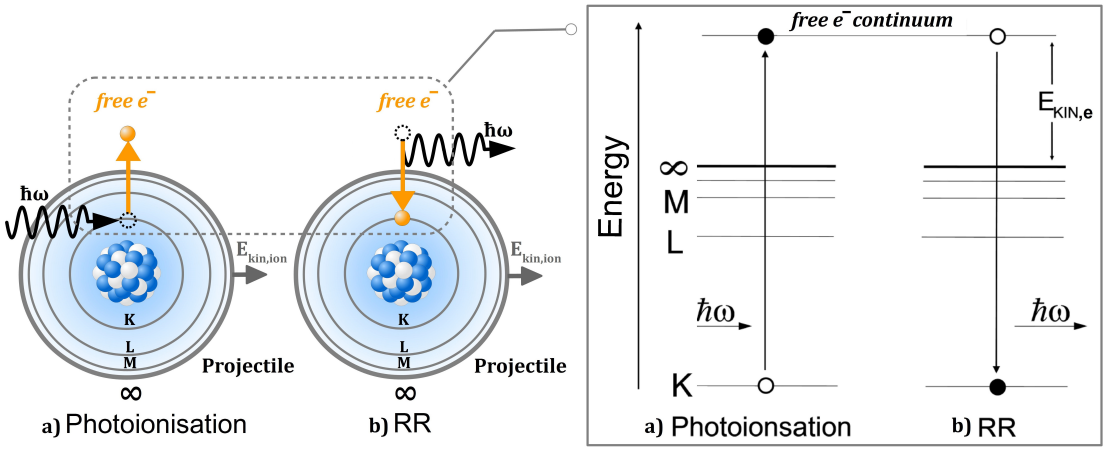

Fig. 5: On the left is a schematic illustration of the radiative recombination process discussed in this work, as well as the photoionization process. On the right is a schematic picture of the change of the energy state of the 'active' electron. Taken from: [25]

REC cross section

The REC process has already been extensively studied experimentally and theoretically and was first identified in the early 1970s by Raisbeck and Yiou [22], by Schnopper et al. [26], and by Kienle et al. [27].

Stobbe presented in 1930 a formalism to calculate the RR cross section in the framework of a non-relativistic dipole approximation [18]. The REC cross section can then be determined (for high non-relativisitic energies) by the described simplification of the REC to the RR process due to the impulse approximation and hence relating it to the photoelectric effect [17]. These calculations give the REC cross section for the radiative electron capture into the K-shell of the projectile. Multiplying the result with the number Z_T of quasi-free electrons in the target yields reasonable results for collision energies up to a few hundred MeV/u, even for high-Z projectiles (e.g. uranium) [28].

The non-relativistic REC cross section scaling dependence is formed by the scaling dependence of the photo-ionization cross section multiplied by the number

of target electrons [28]:

$$\sigma_{REC} \propto \frac{Z_P^5 Z_T}{E_{kin}^{7/2}} \tag{3}$$

A fully relativistic formalism was presented by Ichihara et al. [17] performing the following calculation steps to determine the REC cross section. First of all the photoelectric differential cross section in the projectile frame is calculated and then converted into the RR cross section. This is folded with the momentum spread that comes from the electronic momentum distribution in the initial target state. All angles, frequencies and cross sections are Lorentz transformed into the laboratory frame and then integrating over all differential cross sections gives the total REC cross section for an electron capture into the K-shell of the projectile [17, 21]. For the L- and M-shell the same formalism was applied to calculate the cross sections, but by letting aside all lower atomic shells for the integration. The REC cross sections for the K-, L-, and M-shells were later tabulated per vacancy for radiative recombination into bare nuclei, by Ichihara and Eichler for electron energies ranging up to the relativistic regime [29]. This dense mesh of cross sections allows the interpolation for projectiles ranging from Z = 1 to Z = 112 and is thus an alternative way to dedicated calculations to determine the total REC cross section for an electron capture into a bare projectile. All cross sections of each orbital multiplied by its respective number of vacancies are added up until the M-shell of the projectile for approximative reasons, since the main contributions come from the lower atomic shells. To determine the REC cross section of a projectile that has already bound electrons, screening can be taken into account by using the Slater rules [16].

2.1.2 Non-radiative Electron Capture (NRC)

The non-radiative electron capture (NRC), or also called 'Coulomb capture', describes the process in which an electron is captured from a bound state of a target atom into a bound state of a projectile ion without emission of a photon [24]. The NRC process is still induced by a three-body interaction, so that energy and momentum conservation are fulfilled. But for this process the third particle involved is the target atom [28]. The excess momentum is taken by the target recoil. However, this is only possible if a given momentum component

in the initial electronic wave function finds its counterpart in the final wave function of a bound state in the projectile, which is displaced in momentum space by $m_e v$, with v being the collision velocity [17]. Thus this capture process becomes more and more probable the larger the overlap of the two momentum distributions is. In the non-relativistic energy regime and if the NRC process is dominated by 1s to 1s transitions, the NRC cross section falls off asymptotically with increasing projectile velocity as v^{-12} [24]. This dependency describes the overlap at the far ends of the 1s momentum distributions in the target and the projectile [17]. For higher energies, where the velocity asymptotically approaches c, the fall of the NRC cross sections is better described by E_{kin}^{-5}, while in the relativistic limit this changes to a E_{kin}^{-1} dependence [28]. The NRC process is illustrated in figure 6.

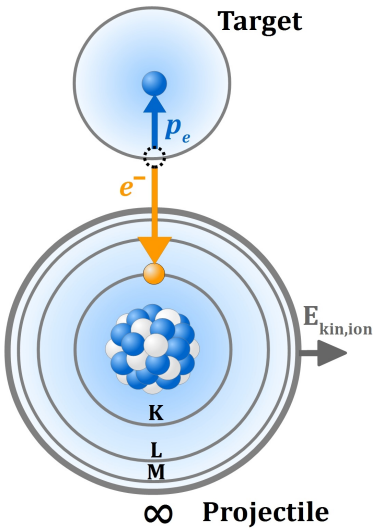

Fig. 6: Schematic illustration of the NRC process: a target electron is captured into a bound state of a projectile while transferring its excess momentum to the target nucleus.

NRC cross section

To determine the NRC cross section in the non-relativistic and in the relativistic framework, Eichler presented an approach based on the eikonal approximation [30, 31] for the electron capture from a hydrogen-like system to the K-shell of a bare nucleus. Compared to the REC process that uses the impulse approximation where the target electron is treated to be free, the captured electron is bound during the NRC process to the target atom and to the projectile ion

at the same time. However, it is very difficult to describe in the theoretical picture the electron correctly with respect to both attraction centres at the same moment. Thus the eikonal approximation is an asymmetric theory treating one electron-nucleus interaction in higher order and the other interaction in first-order perturbation theory. Since it can be either the binding to the target or to the projectile that is taken into account only in an approximate way, there are two versions of this approach called 'prior' and 'post'. The prior version treats the electron-projectile interaction in first order and the electron-target interaction approximately in all orders of perturbation theory. It has been shown [32, 33] that in this version the electron is described having a hard collision with the projectile nucleus followed by multiple soft collision with the target nucleus [34]. The post version treats the interactions the other way around, and thus the electron is having a hard collision with the target nucleus, preceded by multiple soft collisions with the projectile nucleus [34]. In the course of this work, the prior and post version of the theory was adopted on a case by case basis, depending on the size of $\frac{Z_P}{n_P}$ relative to $\frac{Z_T}{n_T}$ for capture from the n_T shell into the n_P shell. Thus, the stronger effective potential is always treated in higher order whereas the weaker potential is treated in first-order.

In the calculations of the eikonal approximation a general cross section formula is first derived, expressed in terms of transformation matrices for initial and final states and in terms of density matrices. Then the density matrices and cross sections for 1s-1s transitions are explicitly calculated, and with the aid of an αZ expansion this formula is cast into an approximate closed-form expression. This density-matrix method can then be generalized to arbitrary initial and final states [30]. A simplified formula for the capture cross section summed of all (n,l) states of specific n_P and n_T was presented by Eichler using hydrogen-like wave functions for the projectile and the target. To expand these electron capture calculations for multi-electron projectiles and targets, the same approximation is done as for the REC cross sections, taking screening effects into account by using an effective charge number Z_{eff} for the nuclei charge.

An appropriate theoretical treatment of the NRC cross section is a real challenge, due to the fact that the atomic wave functions in the target are getting distorted by the Coulomb field of the projectile even at infinite distances. However, the non-relativistic cross section scaling dependence can already be explained

in the first order Oppenheimer-Brinkman-Kramers (OBK) approximation, that gives [28]:

$$\sigma_{\mathrm{NRC}} \propto \frac{Z_P^5 Z_T^5}{E_{\mathrm{kin}}^5} \tag{4}$$

Discussion of electron capture processes

As can be derived from the scaling behaviour of the electron capture cross sections (3) and (4), the NRC drops off rapidly with increasing collision energy as the overlap of the momentum distributions of the initial state in the target atom and the final state in the projectile ion is reduced. However, for the same reason the broader momentum distribution of strongly bound electrons in high-Z targets results in a strong increase of the cross section with increasing target atomic number Z_T. In contrast the REC cross section has a slower decrease with increasing collision energy and exhibits only a linear dependence with the atomic number of the target. These relations can be seen in figure 7, where the REC (dotted line) and the NRC (dashed line) cross sections are shown, as well as the resulting total electron-capture cross sections (solid line) that are compared to experimental data (solid symbols). The prediction for the REC cross sections is obtained within the dipole approximation and for the NRC cross sections by the eikonal approach [30, 31]. In figure 7a the solid circles are the total electron-capture cross sections for U^{92+} colliding with a N_2 target. In figure 7b the solid circles represent the total electron-capture cross sections for U^{92+} on solid targets (Be, C), while the solid squares show the total electron-cross sections of U^{92+} on gaseous targets (N_2, Ar).

The two variables energy and target nuclear charge are allowing four possible scenarios in which the REC and NRC process are having different relative weight. First for low energies and low-Z targets, the processes are competing with each other being of similar relevance. The few target electrons can be captured by either emitting a photon (REC) or by giving energy to the target atom recoil (NRC). If the target atom is heavier and has more bound electrons that can potentially be captured, the electron capture probability increases, with the NRC process outpacing the REC process. As a consequence, there exists a target Z above which, for a given collision energy the total electron capture cross section is dominated by NRC, while below this Z the REC process

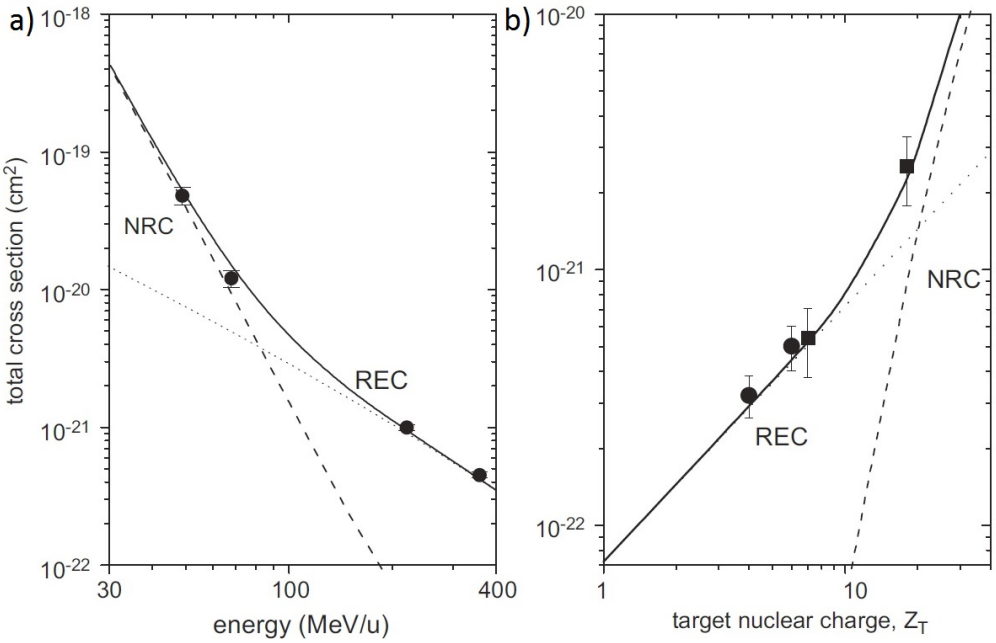

Fig. 7: The NRC cross sections (dashed line), REC cross sections (dotted line) and the total electron-capture cross sections (solid line) that refer to the sum of both predictions and is compared to experimental data from [35]: a) for U^{92+} on a N_2 target versus projectile energy; b) for U^{92+} at 295 $^{MeV}/_{u}$ colliding with gaseous targets: solid squares ($U^{92+} \rightarrow N_2, Ar$) and with solid targets: solid circles ($U^{92+} \rightarrow Be, C$). For N_2 the cross section per atom is given. Taken from: [24]

is more important. In contrast at low collision energies, NRC can completely take over the capture cross section.

For relativistic energies a change for the electron capture cross sections was observed and calculated. The scaling dependences in the relativistic regime follow from the scaling formulas (3), and (4). As presented by Krause et al., the REC and NRC cross sections are scaling approximately with $\sim {}^{Z_T}/_{\gamma}$, respectively with $\sim {}^{Z_T^5}/_{\gamma}$ [36]. In the ultra-relativistic energy regime however, these capture processes are no longer important. Instead the electron capture becomes dominated by another process: the pair production. At very high energies a strong electromagnetic pulse is produced when the projectile ion passes near the target nucleus. This pulse may induce the excitation of an electron, bound in the negative-energy continuum called 'Dirac sea', into a positive energy state [37, 38]. The electron is leaving a hole behind which

acts as a particle with the opposite charge. This way a positron is created. During the production of electron-positron-pairs the created electron may immediately be bound to an unoccupied energetic state of the ion. This electron capture process accompanied by the emission of a positron is referred to as electron capture from pair-production (ECPP) and scales roughly with $\sim Z_T^2 \ln\gamma$ [36, 38, 39, 40, 41, 42].

2.1.3 Ionization

The process where a projectile loses an electron due to Coulomb interaction with either the target electron or the target nucleus is called 'projectile ionization'. When an ion projectile passes a stripper foil, projectile electrons may interact with the Coulomb fields of the stripper atoms. This Coulomb interaction can be described within first-order time-dependent perturbation theory [43], by using the plane-wave Born approximation (PWBA) for single-electron ionizations of projectiles with non-relativistic kinetic energies. This approximation allows treating the collision with the target nuclear charge as only causing an electronic perturbation of the projectile atomic wave function and assumes the projectile trajectory is not disturbed by the collision [28]. However, to describe the ionization process for relativistic energies, including relativistic (magnetic) ion atom interaction, there are theoretical expansions necessary, as will be explained in the next section. The ionization process is illustrated in figure 8.

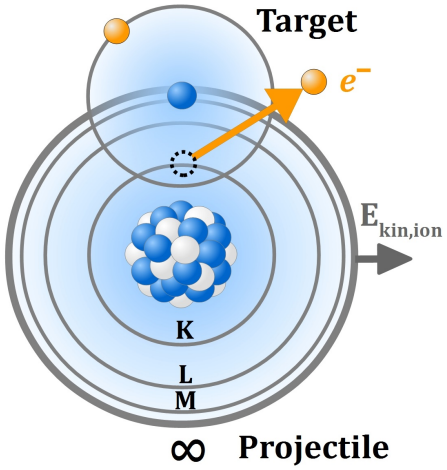

Fig. 8: Schematic picture of the ionization process.

Ionization cross section

To determine the total single electron loss cross section for arbitrary ions in collision with arbitrary targets, Tolstikhina et al. [44] presented the RICODE-M computer programme, that is a product of constant enhancement studies of its predecessor codes that will be explained in the following in a chronological order. The LOSS code presented in [45, 46], was developed to describe the single electron loss cross sections in the non-relativistic Born approximation using the non-relativistic radial wave functions to describe the bound and continuum states of the 'active' projectile electron. These wave functions are obtained by the numerical solution of the Schrödinger equation with the effective field of the atomic core [46], while for the target electron wave functions the node-less analytical Slater functions are used [43]. The LOSS-R-code (Relativistic LOSS code) is an extension of the LOSS code for relativistic energies but still without the relativistic (magnetic) interaction between colliding particles [47].

To improve the LOSS-R code for relativistic ionization of the projectile, the relativistic (magnetic) part of the interaction must be included into the ionization matrix element which in general has the form:

$$M_{if} = \langle f|(1 - \beta\alpha_z)e^{iqr}|i\rangle, \tag{5}$$

with $\beta = v/c$ being the relativistic factor, where c is the speed of light, q is denoting the momentum transfer, α_z the z-component of the Dirac matrix α, and $|i\rangle$ and $|f\rangle$ are the total wave functions of the colliding system in the initial and the final states, respectively [48]. Baur et al. [49] presented the general formulas of ionization cross sections for high energy ion-atom collisions including these magnetic interactions between the colliding particles by using this matrix element (5) and by separating radial and angular parts. This leads to the following form of the ionization cross section [49, 44]:

$$\sigma_{EL}(v) = \frac{8\pi a_0^2 N_{nl}}{v^2} \int_{q_0}^{\infty} Z_T^2(q)\frac{dq}{q^3} \times \left(|F(q)|^2 + \frac{\beta^2(1 - q_0^2/q^2)}{(1 - \beta^2 q_0^2/q^2)^2}|G(q)|^2\right), \tag{6}$$

with $a_0 \approx 0.5292 \cdot 10^{-8}$ cm being the Bohr radius, $v = \beta c$ the ion velocity, N_{nl} the number of equivalent electrons for the principal quantum number n and the orbital quantum number l of the projectile electron shell with the ionization potential I_{nl}. The effective charge of the target is denoted by Z_T,

and is depending on the momentum transfer q and the minimal momentum transfer $q_0 = {}^{(I_{nl}+\epsilon)}/_{v}$, with ϵ being the energy of the ejected electron. F(q) and G(q) are the matrix elements given by $F(q) = \langle f|e^{iqz}|i\rangle$ and $G(q) = \langle f|\alpha_x e^{iqz}|i\rangle$ [50].

Thus, the ionization cross section is composed of the usual Born approximation matrix element $|F(q)|^2$ used for non-relativistic collisions and the relativistic term $|G(q)|^2$ corresponding to the relativistic Born approximation responsible for the magnetic interactions.
Finally the general structure of the RICODE serves as base for the RICODE-M programme (Relativistic Ionization RICODE Modified) that has one important difference: it generates relativistic radial wave functions for the bound and continuous states of the projectile electron, relevant to improve the accuracy for strongly bound electrons in highly-charged (i.e. H- or He-like) high-Z ions [44].

While in the non-relativistic framework, the electron capture and loss processes are competing processes where the REC cross section is depending on (3) and the NRC cross section on (4), the dependence of the ionization cross section derived in the Born approximation is instead given by :

$$\sigma_{EL} \propto Z_T^2 + Z_T, \tag{7}$$

This scaling law is valid for collisions at small impact parameters, where the interaction of the projectile electron with the target nucleus and with the electrons can be treated as separate interactions. However, for large impact parameters the K-shell of the target contributes significantly to the projectile ionization cross section. In this case the non-vanishing electron density between the projectile electron and the target nucleus leads to a screening effect. This screening effect may vary from case to case as presented e.g. in [43, 48], where scaling laws between $Z^{1.45}$ and $Z^{1.8}$ are reported.

Ionization cross sections for relativistic energies
For this work calculations have been done for ions moving with energies of 2.7 GeV/u respectively 5.9 GeV/u. Hence it is important to consider relativistic effects, which has been subject of many studies for the ionization process (e.g. [36, 41, 51, 52, 49, 53]). In the following some effects and their influence on the

ionization cross section will shortly be discussed.

While for high energies the fully non-relativistic cross sections decrease according to Born's asymptotic law with $\frac{\ln(E)}{E}$, the fully relativistic cross sections exhibit a quasiconstant behavior for E > 200 MeV/u (see figure 9) [44].

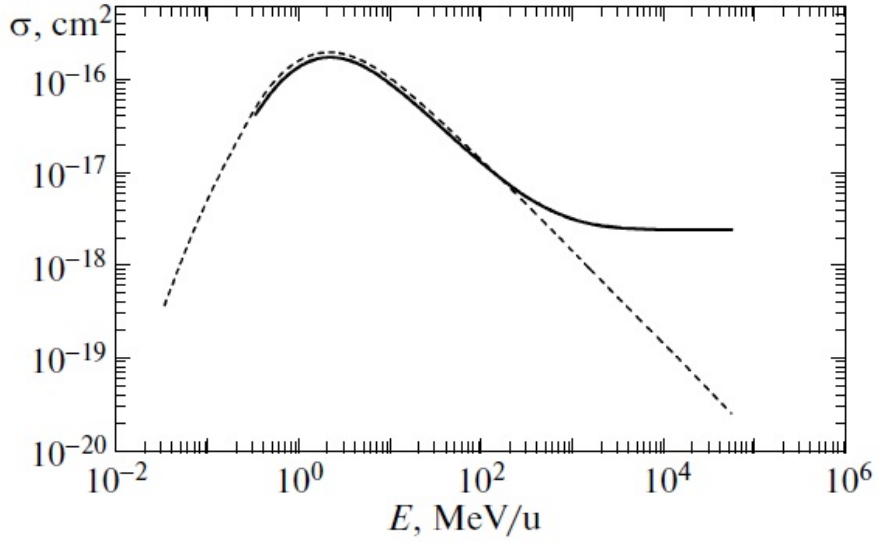

Fig. 9: RICODE-M results of the total electron-loss cross sections calculated with fully relativistic approximations (solid line) for U^{28+} ions in collisions with Ar atoms as a function of the ion energy compared to results for the non-relativistic approximations (dashed line). Taken from: [44]

In the projectile frame, the neutral target atom is moving towards the ion with constant relativistic energy. Describing the case of a collision where the projectile passes near the nucleus, the core potential of the atom is not fully screened by its surrounding electrons, allowing interaction between the projectile electron and the target nucleus. Due to the relativistic energy the electric field of the target nucleus and its electrons has to be described by a so called 'retarding potential', as following. If a charge is moving with a constant velocity near the speed of light, its radial electric field changes its shape: the field lines that radiate directly out of the charge are spread out behind and ahead of the charge and are squeezed together around the sides, as can be seen in picture b of figure 10. This results in a reduced electric field in the longitudinal direction and an increased field in the transversal direction [58]. The latter spans a radial interaction area ($\pi r^2_{\text{Interaction}}$) for the projectile electrons, that increases with the energy. This leads to the conclusion that the ionization

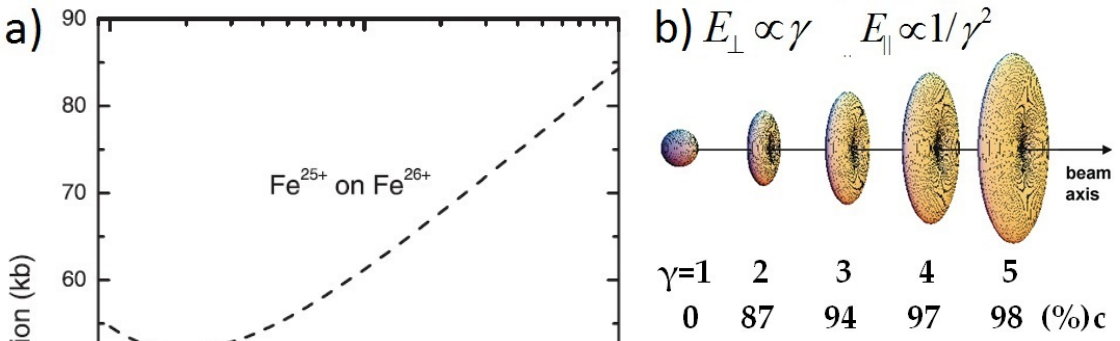

Fig. 10: On the left (a): cross section for electron loss from Fe^{25+} projectile ions on bare Fe ions, neutral Fe and He atoms in function of the projectile energy. Taken from: [54] On the right (b): angular dependence of the electric radial field strengths of a naked target ion as observed in the projectile frame. Perpendicular to the trajectory the electric field steadily increases with γ, while along the direction of motion, it decreases by a factor of γ^2 [55, 56]. Taken from: [57]

cross section also increases for higher γ values. However, since the atom's nucleus is not the only moving charge, the same effect has to be taken into account for the atomic electrons. The transversal electric field of each electron is then also increasing with γ, up to a certain point, where these fields start to overlap with the nucleus charge. This leads to a cancelling effect, which limits the field strength of the nucleus and thus the ionization cross section. In this case the cross section reaches a constant, as illustrated in picture a of figure 10 for collisions of Fe^{25+} with Fe and with He atoms. In the case of naked target atoms without the mentioned screening effect due to the target electrons, the ionization cross section increases with logarithmic behaviour. This can be observed in picture a of figure 10, where Fe^{25+} are colliding with naked Fe ions.

Since passing of ion beams through stripper foils is also always accompanied by energy loss, this effect will be described in the next section.

2.2 Energy Loss

For heavy particles penetrating through matter the inelastic collisions with the atomic target electrons are almost solely responsible for the energy loss. This is caused by the fact, that heavy particles are hardly losing energy by emitting bremsstrahlung. In each of these collisions the ion transfers a very small fraction of its total kinetic energy to the respective target atom, causing atomic electrons to be excited to higher energy states or to be ionized [15].

As along a macroscopic path length there is a very large number of such collisions happening, the overall characteristics of energy loss and also angular straggling of an ion beam are subject to only minor statistical fluctuations. Thus, it is justified to describe the observed energy loss by the stopping power $-dE/dx$. While N. Bohr first calculated this quantity with classical arguments, it was later treated by H. Bethe and F. Bloch using quantum mechanics, resulting in the following Bethe-Bloch-Formula [15]:

$$-\frac{dE}{dx} = 2\pi N_A r_e^2 m_e c^2 \rho \frac{Z_T}{A}\frac{z^2}{\beta^2}\left[\ln\left(\frac{2m_e\gamma^2 v^2 W_{max}}{I^2}\right) - 2\beta^2\right], \tag{8}$$

with $2\pi N_A r_e^2 m_e c^2 = 0.1535\ \mathrm{MeVcm^2/g}$.

r_e: classical eclectron radius = $2.817\text{x}10^{-13}$cm	z: charge of incident particle in units of e
m_e: electron mass	$\beta = v/c$ of the incident particle
N_A: Avogadro's number = $6.022\text{x}10^{23}\mathrm{mol}^{-1}$	$\gamma = 1/\sqrt{1-\beta^2}$
I: mean excitation potential	δ: density correction
Z_T: atomic number of absorbing material	W_{max}: maximum energy transfer in a single collision
A: atomic weight of absorbing material	ρ: density of absorbing material

As can be seen in figure 11, for non-relativistic energies the stopping power is rapidly growing for decreasing energies. Not shown is the very low energy region, where the stopping power has its maximum, when the projectile velocity is comparable to the velocity of the target material electrons. However, directly below the maximum energy loss the stopping power would drop sharply due to several effects. The most important is that the projectile ion captures electrons, leading to a reduced charge and as a consequence also to a reduced stopping power.
For increasing energies, starting in the non-relativistic regime in figure 11, the stopping power is decreasing until the projectile velocity is reaching

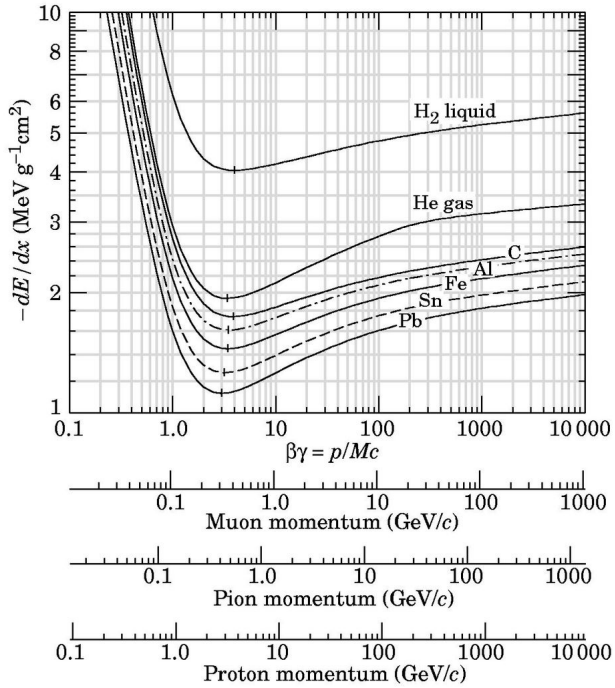

Fig. 11: Stopping power according to the projectile energy calculated by the Bethe-Bloch-Formula (8) plotted versus the momentum of different particles. Taken from: [59]

about v = 0.96 c. Near this velocity particles are called 'minimum ionizing particles' (MIP), since their stopping power is minimal at this point. This is true for almost all particles of the same charge, as can be seen in figure 11. For increasing energies higher than this minimum, the velocity stays almost constant, while the energy loss starts to grow again logarithmically. This comes from relativistic effects as described in the previous chapter for the case of ionization cross sections. However, this rise becomes reduced by the density correction [60].

Above 30 MeV/u the stopping power can be calculated with the on-line application of a programme developed at GSI called ATIMA [61]. This programme includes the theory of Lindhard and Soerensen, which has close connection to the Bethe-Bloch-Formula (8), but includes several correction terms, as it is described in [62, 63].

3 Calculations of Charge State Distributions

If an ion beam is passing through a stripper foil, the interactions between each ion and the target atoms accompanied by charge exchange can differ. The outcome of each collision depends on the corresponding charge-exchange-cross sections. The large multitude of possible process sequences is leading to a variety of different charge states behind the target. All ions with the same charge state q can be taken together as fraction $F_q(x)$. The respective charge state fractions can change with increasing target thickness x, until the so called 'equilibrium thickness' x_{eq} is reached. From this point onwards the 'equilibrium charge-state fractions' $F_q(\infty)$, as well as the mean charge

$$\bar{q} = \sum_q q F_q(\infty) \tag{9}$$

do not change any more with increasing target thickness. These equilibrium charge-state fractions are in fact independent of the initial charge state of the incident ions [64]. Here it is assumed that the kinetic energy of the ion beam which determines the absolute and relative electron loss and capture cross sections does not change significantly during the passage of the target. For targets, thinner than the equilibrium thickness, their charge state fractions are referred to as 'non-equilibrium charge state fractions'. The mean equilibrium charge states of projectiles ranging from protons to uranium can be determined with semi-empirical formulas, e.g. as presented by Schiwietz and Grande [65]. If however, the equilibrium charge state fractions are known, equilibrium charge states can be determined by the analytical equation (9). However, such formulas are based on experimental data sets that may not cover all necessary parameters, like number of charge states or beam energies, to do calculations for specific tasks. This is in particular true for stripping scenarios at new facilities that aim to address parameter ranges where already existing experimental data is sparse or non-existent. Here it is necessary to calculate the charge state evolution of ion beams based on cross sections for the various charge-changing processes.

The evolution of the non-equilibrium charge-state fractions $F_q(x)$ of ion projectiles passing through gaseous or solid targets can be determined by solving the following first-order differential balance rate equations [66]:

$$\frac{dF_q(x)}{dx} = \sum_{q' \neq q} F_{q'}(x)\sigma_{q'q} - F_q(x) \sum_{q' \neq q} \sigma_{qq'}, \tag{10}$$

$$\text{where} \sum_q F_q(x) = 1, \tag{11}$$

with x being either the areal density of the target particles or the target thickness, depending on the target state being gaseous or solid and σ_{ij} the described single- and multi-electron capture ($i > j$) and loss ($i < j$) cross sections, respectively. The equilibrium charge state fractions are obtained by setting the equations to $\frac{dF_q(x)}{dx} = 0$, as treated in detail by Betz [66]. Based on these equations and by neglecting multiple processes a simple analytical formula can be derived, as shown for example by Scheidenberger et al. [28].

The non-equilibrium and also the equilibrium charge state distributions can be determined using different computer codes. The codes used in this work will be presented in the following, as well as their respective calculation method to solve the charge state fraction equations, and their particular limitations. Then will be described which input parameters are necessary for the calculations and for the programmes to perform the calculations as they were done for this work.

3.1 Codes for Charge State Evolution

The used codes are partly open access free-ware and partly internal GSI codes available on request that may become open access in the future. The CHARGE code (version 1.3 from 2003) is developed by Stöhlker et al., at GSI [28] and the GLOBAL code (version 3.9 from 2016) originally developed by Meyerhof et al. at GSI [28]. Both codes can be downloaded for installation from the webpage of Helmut Weick from the GSI (see [67] for further information). In addition they both are implemented into the programme LISE^{++} developed by Tarasov and Bazin of the the LISE group at National Superconducting Cyclotron Laboratory and Michigan State University. The programme is developed to calculate the transmission and yields of fragments produced and collected in a fragment separator and is available for download in [68]. However the CHARGE code was updated in 2006 to take into account relativistic effects in the REC calculations by replacing the Stobbe formula [18] with the fully relativistic formalism

developed by Ichihara et al. [17], as described in section (2.1.1). At the moment this newer version is only available for GSI interns. The BREIT code developed by Winckler et al. at GSI [64] is downloadable for local installation on Linux or MAC OS X, as described in [69], or can be used from any platform via a webpage (see [70]).

CHARGE

As shown already in 1958 by Allison [71] the equations (10) and (11) can be solved analytically for three-state systems. The CHARGE code uses these analytical solutions, restricting it to high-energy charge state distributions for bare, H-, and He-like projectile ions colliding with neutral target atoms. The ionization cross sections for the K-shell are calculated within first order perturbation theory by non-relativistic PWBA. In addition the effect of relativistic binding energies is taken into account and the transverse ionization contribution at relativistic collision energies is approximated, both introduced by Anholt [72]. It should be mentioned, that this method uses relativistic correction terms but no relativistic wave functions. However this simple approximation model, in which relativistic effects are considered, is in good accordance with experimental data from the high energy regime, e.g. for H-like Au ions at 11 GeV/u [73] as described in [28]. Screening effects of the projectile potential can be taken into account by the Slater rules [16]. The NRC cross sections come from the explained eikonal approximation of Eichler [30, 31] by summing up over all projectile shells up to $n = 10$ as well as over all target shells up to $n = 3$ [28]. As already mentioned, the REC cross sections are provided by the fully relativistic formalism developed by Ichihara et al. [17] but only for K-REC. In CHARGE also rough estimates for double processes are covering the two electron exchange processes between the bare and the He-like charge state. The double electron capture cross section is approximated to be 10% of the NRC cross section into bare projectiles, and the double ionization cross section to be 10% of the single-ionization of the H-like projectile [28].
The necessary input parameter to perform calculations with the CHARGE code are: the projectile nucleus charge Z_P, the target nucleus charge Z_T, the projectile kinetic energy E_{kin} in MeV/u, the initial number of electrons $Z - Q = 0, 1, 2$ and the target thickness in mg/cm^2. CHARGE gives as results the non-equilibrium and the equilibrium charge state distributions, as well as the equilibrium target thickness and the calculated cross sections for single and double electron

loss and electron capture, i.e. REC and NRC, for each possible change in charge state. The restriction on three charge states is not the only limitation of CHARGE. The code is developed for high energy collisions and though the minimum energy has to be at least a few ten of MeV/u. At the same time for heavy ions at high energies relativistic effects play an important role. These are taken into account for the REC cross sections, but not for the ionization cross sections that are calculated with non-relativistic wave functions. However, as already described, the comparison with measured data of H-like Au ions at 11 GeV/u [73] shows that these ionization cross sections are still applicable [28].

GLOBAL

To take into account more than three charge states the equations (10) and (11) have to be solved numerically. This can be done by using the Runge-Kutta method, as described by Betz [66]. The GLOBAL code covers projectiles with a maximum energy of 2000 MeV/u, and with 0 up to 28 electrons, corresponding to fully occupied K-, and L-shells and M-shells occupied with all except one electron. For its calculations it uses single-electron loss and capture cross sections. The so called 'stripping cross section' which accounts for electron loss, is determined by the following equation [28]:

$$\sigma(\text{n,n-1}) = n_K \sigma_K^l + n_L \sigma_L^l + n_M \sigma_M^l, \tag{12}$$

while the so called 'attachement cross section' for electron capture is given by the equation:

$$\sigma(\text{n,n+1}) = \frac{2 - n_K}{2}\sigma_K^c + \frac{8 - n_L}{8}\sigma_L^c + \frac{18 - n_M}{18}\sigma_M^c + \sigma_H^c. \tag{13}$$

To calculate the cross section describing the ionization process, equation (12) is used, where the respective ionization cross sections for the different shells are determined again by non-relativistic PWBA in a similar way as in the CHARGE code. However to take also the M- and N-shell, or their respective sub-shells into consideration, the K-shell binding energy is replaced by the binding energy of the respective shell, or sub-shell taken from [74]. GLOBAL takes screening into account by linear interpolation of each σ_X^l between its 'unscreended' value and its 'screened' value, if all shells are filled with electrons [28]. In addition it also takes double K- and L-shell ionization into account schematically, as described in [75]. The cross section describing the electron capture process is

calculated by equation (13). It is solved by calculating and summing up the non-radiative and the radiative capture cross sections. The eikonal approximation is also used in GLOBAL to compute the non-radiative ones σ_X^c, by using the analytical formula for the K-shell [30, 31], and adapting it to the other shells as described in [34]. However, instead of summing up over 10 projectile shells and 3 target shells as in CHARGE, it is only summing up over 3 projectile shells and 3 target shells. For the radiative cross section an average value of the Sauter and the Bethe-Salpeter cross sections is used [21, 28]. In GLOBAL are also considered the double and triple capture schematically, using [75]. In addition, it also takes the slowing-down of particles into account. This is an advantage over the CHARGE code, which neglects the energy loss, and the reason which makes the GLOBAL code very suitable for the middle energy regime, where for thick targets the energy loss can have an influence on the cross sections. The CHARGE code however, doesn't need this feature since it is mainly used for heavy ions in the high energy regime (above the upper energy limit of GLOBAL of 2000 MeV/u), where the energy loss can be neglected compared to the projectile energy [28].
The input parameters necessary to compute the charge state distributions with GLOBAL are mainly similar as for CHARGE: the projectile nucleus charge Z_P, the target nucleus charge Z_T, the projectile kinetic energy E_{kin} in MeV/u, and the electron number, or the initial number of electrons $Z - Q$ that can go up to 28 electrons for GLOBAL, as well as the target thickness in mg/cm^2. In addition, GLOBAL has the feature by taking into account the energy loss, to calculate for a given end energy the required target thickness. Then for this thickness it calculates the charge state distribution. So it not only allows the determination of the charge state distribution with the input of an initial projectile energy, but also with a projectile's end energy.

BREIT

This recently developed programme allows to solve the equations (10) and (11) in an analytic form using the eigenvalue decomposition and matrix inversion method [64], that is presented for example by Strang [76]. One of the most important differences compared to the other available programmes for charge state distribution calculations is that it has no built-in cross sections. This allows it to determine the charge state distributions with full control over the input cross sections, as these needs to be supplied by the user. Thus the

accuracy of the calculations of the BREIT code are restricted by the availability and quality of the different cross sections for each charge exchange process.

To perform the calculations with the BREIT code for this work, the cross sections were calculated for each single-electron charge exchange. The calculations of these cross sections were performed using the treatments described in section (2.1): the electron loss cross sections for the L- and M-shell are calculated and provided with the RICODE-M code by V.P. Shevelko, while the K-shell ionization cross section is determined by CHARGE. The REC cross sections are obtained by interpolation with respect to a screened effective nucleus charge state, over the tabulated exact REC cross sections per vacancy, calculated by the fully relativistic formalism presented by Ichihara et al. . For the NRC cross sections the eikonal approximation of Eichler is used [30, 31], summing up over all projectile shells up to $n = 50$ and target shells $n = 3$, while taking into account the screening by projectile and target electrons.
The necessary input parameters for the BREIT code are imported in an input file. This file has to contain the projectile nucleus charge Z_P, the target nucleus charge Z_T, the target mass number A, the projectile E_{kin} in MeV/u, the target thickness in mg/cm^2, as well as the cross sections for at least all the possible single-electron charge exchange processes between the charge states of interest. The multi-electron processes could also be taken into account. However, since the cross sections for this work only rely on the single electron approximation, these were neglected, with exception of the double loss and capture processes inside the K-shell of the projectile, that are approximated just as in the CHARGE code [28].

4 Results and Predictions

The main goal of the studies made for GSI and CERN is to find a convenient stripper target material and stripper target thickness to produce the highest possible fraction of the desired charge state for a given energy and projectile ion. The programmes described above were used depending on their functionality and advantages. If only three charge states are relevant for the projectile, CHARGE can be used to calculate the charge state distribution analytically. For many-electron systems the GLOBAL programme can be used to make predictions for up to 28 electrons. However, this programme only operates for energies up to 2 GeV/u. Since the beam energies considered for projectile stripping at the upcoming facilities are surpassing this limit, the calculations in the high energy regime were performed with the BREIT code. The used models for the calculation of the cross sections for the charge exchange processes are all taking into account relativistic effects. Furthermore they are allowing the analytical determination of the charge state distribution for all elements in the periodic table, if the necessary cross sections are available. Finally, for the studies in this work the described programmes were used as following: for high energies the BREIT code was used, for lower energies GLOBAL, and just for comparison at high energies also CHARGE was used to determine the charge state distributions.

In the following will be presented the charge state predictions for the FAIR facility at GSI, as well as for the Gamma Factory for CERN.

4.1 Studies for the FAIR Facility at GSI

This first study represents an example, where the BREIT code, in combination with the described cross sections for ionization, as well as for radiative and non-radiative capture, is applied to a stripping scenario at the future FAIR facility. As described at the beginning of this work, it will be possible to accelerate U^{28+} up to $\sim$ 2700 MeV/u in the SIS100. Due to its availability in the future, this energy and projectile have been chosen for this study, where the goal is to find the ideal stripper material and thickness to produce an ion beam of U^{89+}. Note that this charge state was not chosen for a special reason, but only to exemplify the application of the BREIT code together with the cross

section models. In this regard, however, it is simply the next highest charge state that the described calculation model newly allows to investigate in this high energy regime, overcoming the previous limitation to U^{90+}, U^{91+} and U^{92+}, which could already be calculated with the commonly used CHARGE code. The studied target materials are spanning the range from ${}^{12}_{6}C$ up to ${}^{207}_{82}Pb$ and were chosen because they are commonly used as stripper targets, due to their functional mechanical properties.

In this case study however, only the strongest bound electrons are taken into account. Therefore the projectile has only a fully occupied K- and L-shell (U^{82+} instead of U^{28+}). As a consequence of this approximation the target thickness does not include the additional thickness that it takes for the ions to lose the other 54 electrons, and the yield would be slightly bigger. However due to the fact, that only single-electron loss is taken into account results in a systematic underestimation of the electron loss. It is well-known that for many-electron projectiles multi-electron loss cross sections can reach up to the same magnitude as the single-electron loss cross sections [48]. The effect of taking into account more electrons in the incident ion charge state will be discussed in more detail later, in the presentation of the results for the CERN scenario.

The BREIT code results for one of the target materials, in this case ${}^{64}_{29}Cu$, can be seen in figure 12, where the fractions of the different charge states are displayed against the target thickness. In this figure is visualized that in this high energy regime, for the ionization of the electrons in higher excited states is needed much less target thickness, as for the ionization of the K-shell electrons. This could already be expected, since the ionization cross sections for the excited electrons are several orders of magnitude bigger. Interesting is also the yield of the respective charge states, which also depends on the probability that an ion with a certain charge state is losing or capturing an electron. It should be mentioned, that since the calculations start witch hundred percent of U^{82+}, also the fraction of U^{82+} (black line) in the graph starts at hundred percent and is only decreasing with the increase of thickness.

To compare the yield and required thickness for different target materials for the production of an U^{89+} ion beam, the respective fraction of each target

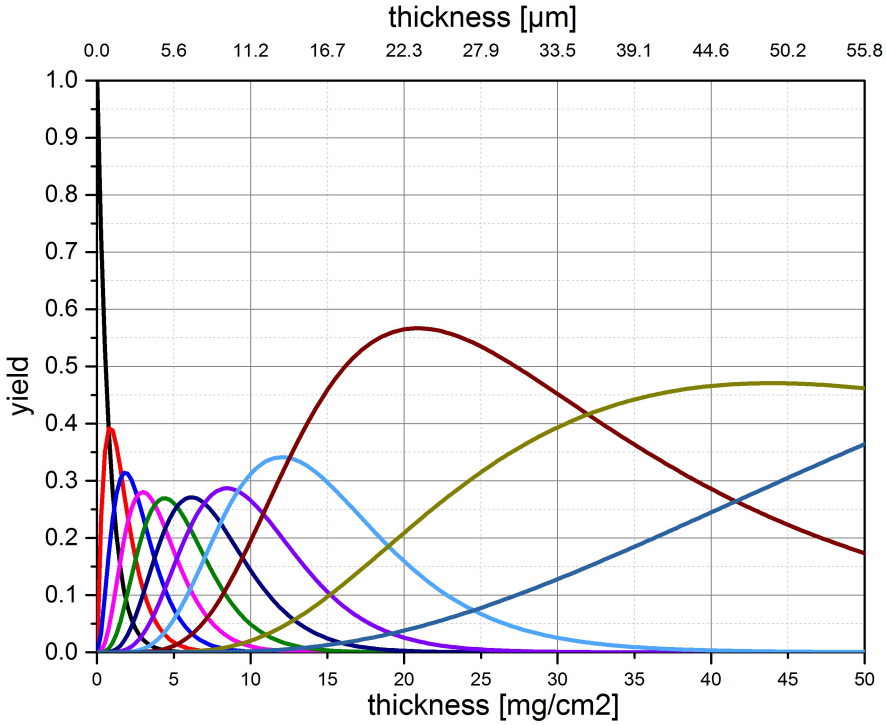

Fig. 12: Charge state distribution after collision of U^{82+} with $^{64}_{29}Cu$ at 2700 MeV/u against the target thickness in mg/cm^2 as well as μm, calculated with the BREIT code. The lines from left to right are corresponding to the yield of the different charge state fractions from U^{82+} up to U^{92+}.

material can be extracted and put into a graph with the fractions calculated with the other materials. The result can be seen in figure 13, where the yield of U^{89+} against the target thickness is displayed for the different target materials. The fraction calculated for $^{64}_{29}Cu$ is represented by the bright blue line in both figures (figure 12 and figure 13). Figure 13 shows that with decreasing nuclear charge of the target Z_T the yield of U^{89+} peaks at higher target thickness. At the same time the target thickness range, in which the highest amounts of U^{89+} can be produced, increases for smaller Z_T. These observations can be explained by the fact, that for low-Z targets, the loss cross sections are much smaller than for high-Z targets, due to its $Z_T^2 + Z_T$ scaling. In addition the electron capture cross sections, dominated by the REC process for high energies, are scaling with Z_T and are therewith much nearer to the ionization cross sections. However in this energy regime the electron loss cross sections are still significantly higher in comparison, and thus the ionization process is dominating.

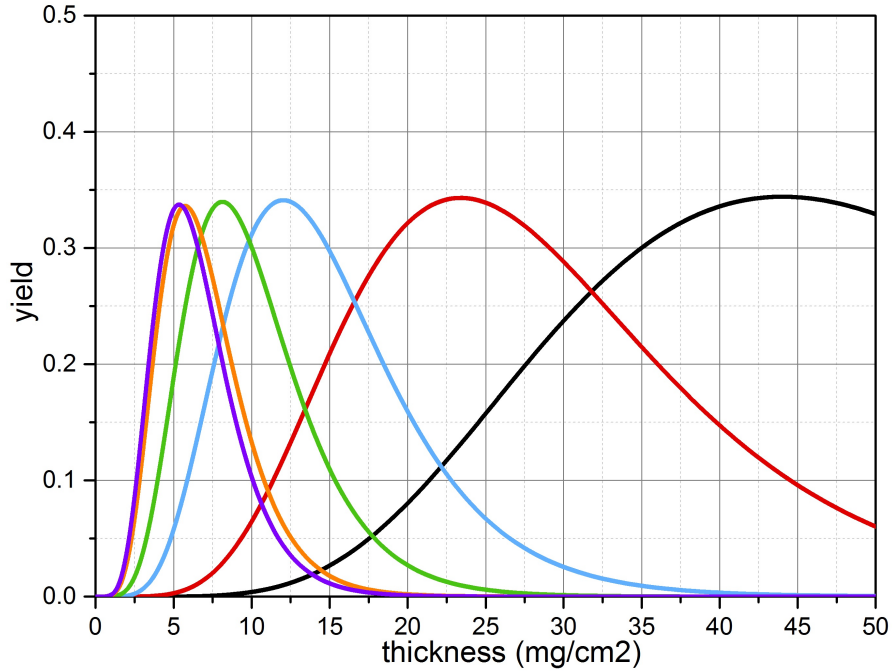

Fig. 13: Yield of U^{89+} after collision of U^{82+} with different target materials at 2700 MeV/u against the target thickness in mg/cm^2, calculated with the BREIT code. The lines from left to right are corresponding to the following target materials: $^{207}_{82}$Pb (violet line), $^{197}_{79}$Au (orange line), $^{108}_{47}$Ag (green line), $^{64}_{29}$Cu (blue line), $^{27}_{13}$Al (red line), $^{12}_{6}$C (black line).

Table 3: Yield of U^{89+} after collision of U^{82+} with different target materials with different thickness at 2700 MeV/u, resulting from figure 13. The energy loss was calculated with ATIMA.

2700 MeV/u U^{82+} on	$^{12}_{6}$**C**	$^{27}_{13}$**Al**	$^{64}_{29}$**Cu**	$^{108}_{47}$**Ag**	$^{197}_{79}$**Au**	$^{207}_{82}$**Pb**
max. yield of U^{89+}	34.41%	34.31%	34.12%	33.98%	33.67%	33.77%
Thickness (mg/cm^2)	44.01	23.51	12.01	8.01	5.76	5.26
Thickness (μm)	194.73	87.11	13.40	7.63	2.98	4.64
Energy loss	0.113%	0.0563%	0.0251%	0.0157%	0.00996%	0.009%

The maximum yields for the different target materials are displayed in table 3, together with the associated target thickness in mg/cm^2 and μm. As can be seen the value of the maximum yield is nearly the same for the different materials in this energy regime. This is due to the fact that the ratio of the

ionization cross sections for the transitions between the different charge states is about the same. And since for such high energy, only the ionization process dominates, the resulting yield is also roughly the same. The choice of the stripper foil in such a case depends strongly on the mechanical feasibility to produce the foil and their ability to sustain the ion bombardment for a reasonable period of time. The long term stability of 4.64 μm of $^{207}_{82}$Pb, or 2.98 μm of $^{197}_{79}$Au, or even 7.63 μm of $^{108}_{47}$Ag is questionable and would have to be investigated by a target laboratory at an accelerator facility. Furthermore the choice of a stripper foil is also depending on the energy loss of the ion beam while passing the target material. This was calculated with the ATIMA programme [61] mentioned in section 2.2, and has also been tabulated for the different target materials in table 3. This programme needs as input parameter the charge state of the projectile. This means that for the determination of the exact energy loss, a stepwise calculation would be necessary to account for the change of the (average) ion charge state as a function of the penetration depth. However, for this work the equilibrium mean charge state was used to calculate the energy loss, resulting in the theoretical extreme case where the energy loss would be maximal. However, at the energy of interest the energy loss for stripper foils of the thickness necessary to produce maximum fractions of U^{89+} is quite small and not worth of a detailed investigation. This can also be seen in table 3, where is tabulated the energy loss for all the target materials. As explained by the Bethe-Bloch-Formula (see formula (8)), the ions tend to have a very small energy loss in the high energy regime.

4.2 Studies for the Gamma Factory at CERN

For the Gamma Factory study, the goal is to find the stripper foil material and thickness to produce most effectively hydrogen- and heliumlike lead ions (Pb^{80+} and Pb^{81+}, respectively) out of Pb^{54+} ions. These charge states will be used as the driver beam of the Gamma Factory as described in chapter 1. The two possible positions of the stripper foil are either at the entry to the PS at 72.2 MeV/u, or in the transfer line from the PS to the SPS at 5900 MeV/u (for details, see figure 3). In the first case the energy is low enough to use the GLOBAL code for the determination of the charge state distribution. This was done with respect to all of the 28 initial projectile electrons. In the second

case the BREIT code had to be used, considering all of the 28 initial electrons of the projectile. In addition, the CHARGE code was used, implying that the initial charge state had to be assumed to be Pb^{80+} instead of Pb^{54+}, to compare its results with the BREIT code predictions. The results of the BREIT/Charge code are shown in the pictures a, b, c, and d of figure 14, and the results of the GLOBAL code in the pictures a, b, c, and d of figure 15.

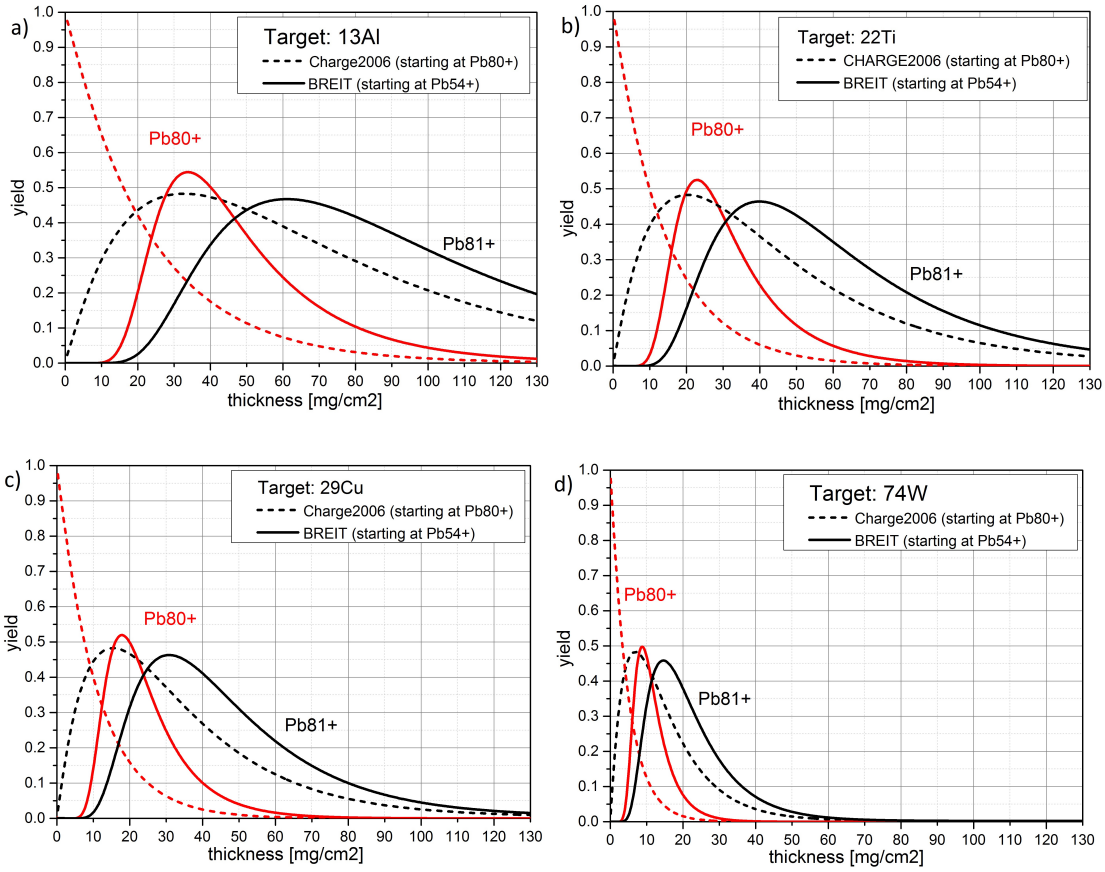

Fig. 14: Yield of Pb^{80+} and Pb^{81+} after collision of Pb^{54+} on different target materials at 5900 MeV/u, calculated with the BREIT code (solid lines) and compared to the results of the CHARGE code (dashed lines).

First of all, the difference between the BREIT code and the CHARGE code results will be shortly explained, in order to avoid any confusion regarding the different graph shapes. It can be seen that for the BREIT code, which takes into account 28 electrons, the yield of Pb^{80+} (red line) rises from 0 up to its maximum, before it starts falling again asymptotically. Here the ions start with Pb^{54+} and reach higher and higher charge states, due to the single

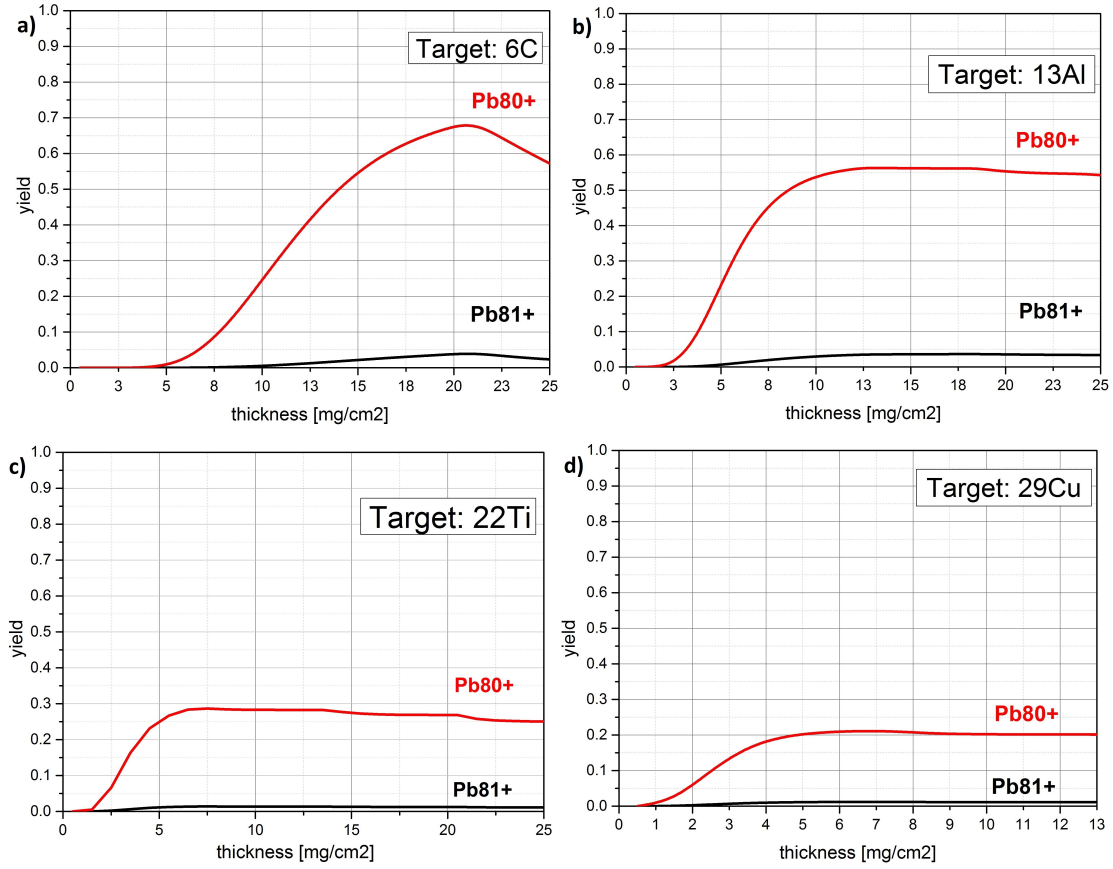

Fig. 15: Yield of Pb^{80+} and Pb^{81+} after collision of Pb^{54+} on different target materials with 72.2 MeV/u, calculated with the GLOBAL code.

electron loss process. So in the beginning there are no ions with Pb^{80+}, until ions that reached Pb^{79+} lose another electron. The CHARGE code however, is only taking three charge states into account, starting with Pb^{80+}. Therefore the respective curve of the CHARGE code (red dashed line) starts already at 100% of Pb^{80+} ions, and only the asymptotic fall of the curve can be seen. With increasing thickness more and more ions lose an electron, reaching the Pb^{81+} charge state. However the exact yield of Pb^{80+} at a certain penetration depth could at best be estimated. While the CHARGE code does not provide an accurate result of the yield of Pb^{80+}, it shows a transition behaviour between the Pb^{80+} and the Pb^{81+} charge states as a function of the target thickness, which is confirmed by the results of the BREIT code. The yield of Pb^{81+} ions can be calculated with both codes, and as can be seen in the pictures of figure 14 the results are very similar. This is no surprise, since the BREIT code also uses the ionization cross sections of CHARGE and nearly the same capture

cross sections. However, the yield calculated with the CHARGE code is slightly higher than calculated with the BREIT code. This can be described by the fact, that when maximum yield of the BREIT code is reached, still a small amount of ions may have a smaller charge state, since the BREIT code is not starting with 100% Pb^{80+}. Aside from the yield, however, the CHARGE code is very limited to predict the necessary target thickness. It is clear that the ions need to pass through a certain thickness to reach Pb^{80+} by single electron loss. For the scenario of the high energy regime however, the exact thickness can be calculated using the BREIT code, which is a big advantage compared to the other codes. Not only does it allow to calculate the yield of Pb^{81+} with higher accuracy, but it also gives an idea of how much thicker the target needs to be, compared to the CHARGE prediction, before reaching the maximum yield of the higher charge states. The BREIT code results of the charge state distribution of Pb^{54+} on $^{64}_{29}Cu$ at 5900 MeV/u are shown in figure 16, where can be seen the thickness, necessary to lose enough electrons to achieve Pb^{80+} ions. In this figure is also shown the very small yield of Pb^{79+} that is the cause for a smaller Pb^{81+} yield compared to the result of the CHARGE code.

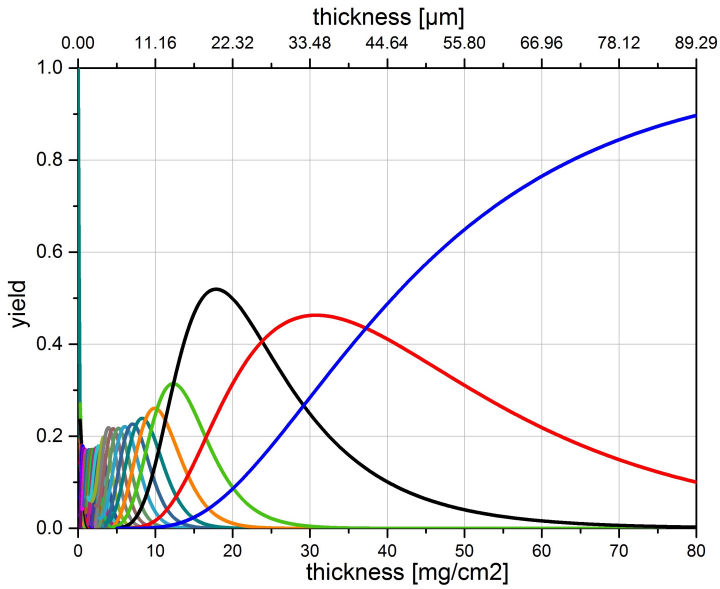

Fig. 16: BREIT code results of the charge state distribution for Pb^{54+} passing through $^{64}_{29}Cu$ at 5900 MeV/u. The lines from left to right are corresponding to the yield of the different charge state fractions from Pb^{54+} up to Pb^{82+}.

As can be seen in figure 16, the necessary thickness to lose an electron is for

Pb^{54+} very small and is then growing for each transition. This comes from the fact, that the ionization cross sections for transitions between smaller charge states are higher than for the transitions between higher charge states. For very high energies the cross sections for transitions in the different shells may vary by several orders of magnitude in size. This magnitude difference is observable in figure 16 by steps in the charge state distribution. The charge state distribution of ions having their valence electron in the L-shell and ions having their valence electron in the M-shell are forming plateaus which are distinguishable from the rest. According to the BREIT code, for the studied materials the thickness has to be about 50% thicker, as the thickness calculated with the CHARGE code.

Before the interpretation of the GLOBAL code and BREIT code results for different target materials, it is important to indicate once again that for an ideal stripper foil aside from the yield, also the energy loss has to be taken into account. It plays an important role since a too high loss of beam energy can be causing a crucial problem in sustaining the ion beam in an accelerator. As could be seen already in the study for the GSI, the energy loss in the high energy regime is very small. In this study however, one of the possible scenarios is to strip the Pb^{54+} ions at 72.2 MeV/u. According to the Bethe-Bloch formula (see formula (8)) ions lose most of their energy in the lower energy regime. With these information will now be succeeded with the interpretation of the results of the charge state distribution calculations for the production of Pb^{80+} or Pb^{81+} for each of the two possible scenarios.

As can be seen for the GLOBAL results (see pictures a, b, c, and d of figure 15), in terms of producing Pb^{80+}, a $^{12}_{6}C$ and a $^{27}_{13}Al$ stripper foil provide with in between 50-70% of the ions a significantly higher yield compared to the yield of $^{48}_{22}Ti$ and $^{64}_{29}Cu$, which lies in between 15-30% . From these studied materials, the $^{12}_{6}C$ target material seems to be the most effective one in achieving the highest amount of ions with the charge state of interest, according to GLOBAL. However, it has the drawback of having a higher loss compared to $^{27}_{13}Al$. Therefore a $^{27}_{13}Al$ foil in the range of about 12.50 mg/cm^2 might be the optimal choice for the production of Pb^{80+} ions at 72.2 MeV/u, due to its lower energy loss, while still providing an acceptable yield. It should be mentioned, that the stability of 6.50 mg/cm^2 (equals 7.29 μm) $^{64}_{29}Cu$ is questionable. But as can be

seen in picture d of figure 14, the foil could also be chosen thicker resulting in roughly the same yield. However, this would increase the energy loss, and the maximum yield would still be too small to make $^{64}_{29}$Cu a preferable target material choice for the production of Pb^{80+}.

For the production of Pb^{80+} ions at 5900 MeV/u, the results of the BREIT code (see pictures a, b, c, and d of figure 14) show that all the studied materials would have a yield in between 45-55%. $^{27}_{13}$Al provides the slightly highest yield, closely followed by $^{48}_{22}$Ti, then by $^{64}_{29}$Cu, and finally by $^{184}_{74}$W, with the lowest yield, which differs about $\sim$ 5% from the yield of $^{27}_{13}$Al. As for the energy loss, the order is the other way round, with $^{184}_{74}$W providing the smallest loss and $^{27}_{13}$Al the biggest. As expected, the energy loss of all the materials is significantly smaller at 5900 MeV/u compared to the results at 72.2 MeV/u. However, the low stability and therewith the short endurance of 8.76 mg/cm^2 (equals 4.55 μm) of $^{184}_{74}$W might be too limited for the use in an accelerator. Hence the foil should be chosen from the other three materials, where normally would have to be pondered how high the energy loss in the accelerator is allowed to be. However, in this case it is marginal for each of the materials and therefore not an important factor for the choice of the stripper foil.

In terms of Pb^{81+}, the results of the GLOBAL code show that stripping at 72.2 MeV/u does not provide an efficient yield for any of the studied materials, since none of them is having a yield of over 5%. Much more promising are the results for the scenario of stripping at 5900 MeV/u. Here the yield mounts up to values in between 40-50%, according to the BREIT code. The highest yield can once again be achieved with $^{27}_{13}$Al, then with $^{48}_{22}$Ti, then $^{64}_{29}$Cu, and then with $^{184}_{74}$W. However, this time the difference between the yields is minuscule, the biggest and smallest amounts are just about $\sim$ 1% apart. The big difference lies in the target thickness compared to the production of Pb^{80+}, which has for some materials almost to be doubled (for details, see table 4, where the results for the different scenarios are tabulated). This leads to an energy loss, that while still being very small, of course is also almost doubled. As turned out, once again the stability of 14.51 mg/cm^2 (equals 7.53 μm) of $^{184}_{74}$W might be too limited for the use in an accelerator. Therefore the $^{184}_{74}$W foil can be dismissed as solution for the production of ions of the charge states of interest.

Table 4: Tabulated values of the respective yield of Pb^{80+} and Pb^{81+}, the target thickness, as well as the energy loss calculated with ATIMA after collision of Pb^{54+} with different target materials with different thickness at 72.2 MeV/u and at 5900 MeV/u, resulting from the pictures of figure 15 and figure 14.

Projectile : Pb^{54+} on Target	$^{12}_{6}$**C**		$^{27}_{13}$**Al**		$^{48}_{22}$**Ti**		$^{64}_{29}$**Cu***	
72.2 MeV/u - charge state	**Pb^{80+}**	**Pb^{81+}**	**Pb^{80+}**	**Pb^{81+}**	**Pb^{80+}**	**Pb^{81+}**	**Pb^{80+}**	**Pb^{81+}**
max. yield	68.207%	3.961%	56.321%	3.650%	28.551%	1.393%	21.151%	1.218%
Thickness (mg/cm^2)	20.50	20.50	12.50	18.50	7.50	7.50	6.50	6.50
Thickness (μm)	90.71	90.71	46.32	68.55	16.52	16.52	7.29	7.29
Energy loss	6.37%	6.37%	3.32%	4.99%	1.80%	1.80%	1.41%	1.41%
Projectile : Pb^{54+} on Target	$^{27}_{13}$**Al**		$^{48}_{22}$**Ti**		$^{64}_{29}$**Cu**		$^{184}_{74}$**W**	
5900 MeV/u - charge state	**Pb^{80+}**	**Pb^{81+}**	**Pb^{80+}**	**Pb^{81+}**	**Pb^{80+}**	**Pb^{81+}**	**Pb^{80+}**	**Pb^{81+}**
max. yield	54.424%	46.739%	52.489%	46.402%	51.948%	46.297%	49.786%	45.847%
Thickness (mg/cm^2)	33.76	61.00	23.01	39.76	17.76	30.75	8.76	14.51
Thickness (μm)	125.09	226.02	50.68	87.58	19.91	34.47	4.55	7.53
Energy loss	0.0346%	0.0625%	0.0217%	0.0375%	0.0159%	0.0276%	0.0066%	0.0109%

*The results for this foil are showing the thinnest possible thickness for maximum yield. However, the foil could also be chosen thicker resulting in roughly the same yield, but inducing higher energy loss.

After the detailed discussion of the calculation results it appeared that there are many parameters, that have to be considered in order to chose the optimal stripper foil. In the ideal case, the stripper foil should provide maximal yield of ions of the charge state of interest, while having minimal energy loss and having most suitable mechanical properties, that provide the best compatibility to the accelerator facility and all processes involved.
The goal of this study is to predict the charge sate distribution, and by that to support the finding of an optimal solution to strip Pb^{54+} to produce efficiently Pb^{80+} and Pb^{81+}. However, in the used programmes many approximations and estimations had to be included, so the results of the calculations should not be understood to represent an absolute and precise value. Instead the results should act to give an idea of what could be expected, according to theories that were tested at multiple other different experiments over the last decades. Therefore, this study should be recognized to be a guideline for the experimental tests, that finally will have to be executed to definitely decide over the stripper foils for the final experimental setup. In this process will have to be tested different materials and different thickness anyway, but this study allows to narrow down the material choices and refers to the respective area

where the test runs should begin to search for the ideal target thickness. As a result of this work $^{27}_{13}$Al and $^{48}_{22}$Ti stripper foils will be tested at CERN. They will be installed in between the PS and SPS accelerators (see transfer line TT2 in figure 3), where the ions will be stripped at 5900 MeV/u. The experimental tests are scheduled for 2018 at CERN.

5 Experimental Determination of Electron Capture into Excited States of Xenon Projectiles

In this chapter a measurement of capture cross sections for a beam of bare xenon ions colliding with a hydrogen gas target will be discussed. The resulting experimental data will serve to verify theories and codes used for the calculation of NRC cross sections. The experiment was performed by Jan Glorius et al. at the ESR storage ring at GSI, Darmstadt with ion beam energies in the range between 5.5 MeV/u and 30.93 MeV/u. This energy range is of particular importance for the future operation of CRYRING@ESR, where highly-charged ions will be used for experiments at velocities much smaller than what is necessary to create their high charge states. This capability to perform measurements with strongly decelerated ion beams is almost unique to GSI, and with the CRYRING@ESR it will be extended to even smaller energies than currently accessible by the ESR (which has a lower energy limit of approximately 4 MeV/u, compared to a few keV/u in the CRYRING@ESR). Currently only very few data exists for capture cross sections of highly-charged, decelerated ions. However, the capture rate will determine ion beam lifetimes in the CRYRING@ESR and is therefore a very important parameter for the planning of future experiments. This raises the interest in additional measurements of charge-changing cross sections of highly charged ions at low energies, as will now be presented in the following.

5.1 Experimental Setup

The experimental data analysed in this work was obtained during a beam time in 2016, which was dedicated to the measurement of the p-γ cross section, which is an important parameter in nuclear astrophysics models. For the experiment, the following experimental setup was used: an interaction chamber was placed inside the beam line of the ESR at GSI. In this chamber a gas target was passing in form of a low pressure gas beam that was inserted from the top inside the chamber. An ion beam of Xe^{54+} was guided from the SIS18 into the ESR, where it was passing the gas beam. An array of standard Ge(i) X-ray detectors was placed at different angles with respect to the ion beam axis, around the interaction zone of the ions with the hydrogen molecules. These detectors allowed to record the X-rays emitted during the occurring collisions, in particular those stemming from radiative capture of target electrons into the

ground state of the projectile ion. The experimental setup is illustrated in figure 17.

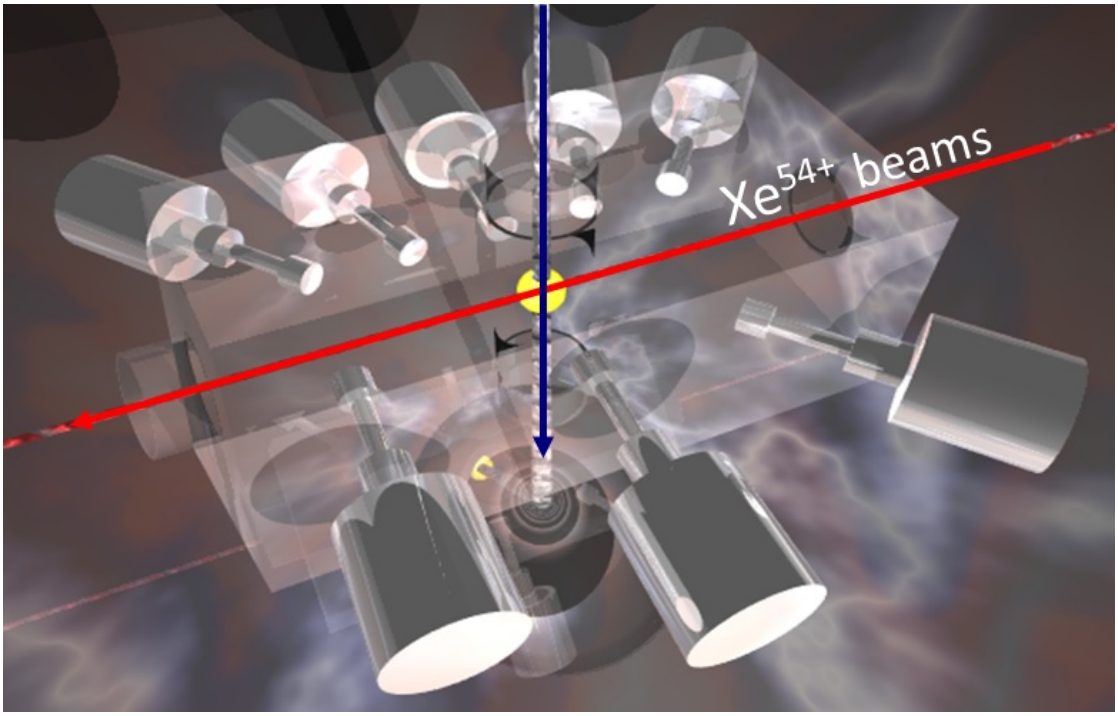

Fig. 17: Experimental setup at the internal gas target for X-ray detection at the ESR at GSI. The transparent box is the interaction chamber, and the cylinders are the germanium detectors positioned at different angles with respect to the central gas target. The Xe^{54+} projectile beam line is pictured as a red line and the hydrogen gas jet is pictured as a blue line. The yellow circle shows the interaction area. Taken from: [77]

While detectors could be placed at multiple positions at the interaction chamber, for the experiment in 2016 only three positions were occupied: at 35°, at 60°, and at 90°. At each position a planar Ge(i) detector was installed with a crystal thickness in the range between 10 up to 20 mm. The concerning detector positions are illustrated in detail in the following sketch (figure 18) of the setup.

The value of the nuclear reaction cross section was obtained by normalizing the count rate of a particle detector, which detects the ions that captured a proton from the gas target, to the well-known cross section of the REC process. In the following analysis the intensity of the K-REC peak is also used for normaliza-

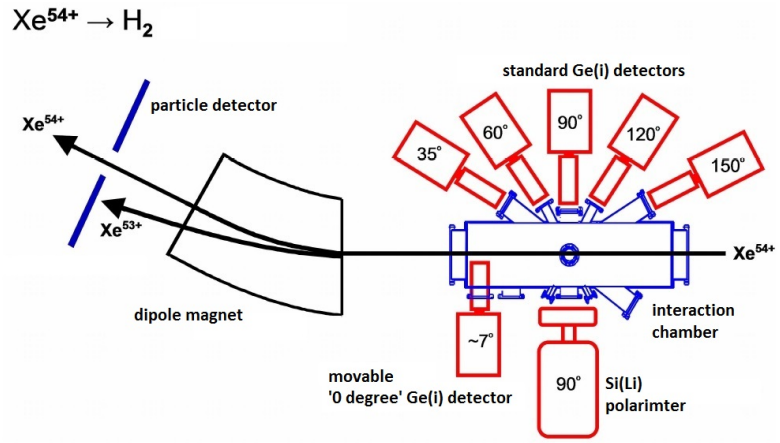

Fig. 18: Sketch of possible detector positions at the interaction chamber for X-ray detection at the internal gas target of the ESR at GSI. For the experiment discussed in this work only the detectors at 35°, at 60°, and at 90° were used. Taken from: [25]

tion. But instead of a nuclear reaction, the cross section of interest is the electron capture cross section in all states higher than the ground state of the projectile. Capture into excited states is followed by nearly instantaneous transitions into lower energetic states and finally the ground state. These processes are accompanied by the emission of photons of characteristic energies. The direct transition of excited states into the ground state results in the emission of Lyman radiation that is also detected by the aforementioned X-ray detectors. By normalizing the Lyman intensity to the intensity of K-REC photons, in combination with the well-known K-REC cross section, it is possible to obtain the total cross section for capture into all excited states, which consists of the NRC and REC contribution.

Assuming that the photon emission due to transitions from excited projectile states to lower lying states is isotropic in the emitter frame allows to estimate the photon yield obtained under a certain angle to represent the mean value in each angular direction. Thus the total electron capture cross sections into shells above the K-shell can be derived. In reality though, the photon count is not measured exactly the same by all detectors, and technical malfunctions may occur. This is why multiple detectors were used, allowing to compare their results. This led to the dismissal of the results of the detector at 90°, since it was not properly adjusted for this study. In addition some measurements with

the detector at 35° were not usable for the analysis, since the trigger threshold was set too high resulting in spectra where characteristic photon peaks were missing (6 MeV/u, 7 MeV/u, 15 MeV/u, and 30.93 MeV/u).

In the following, the method and the results of the analysis of the experimental data will be presented.

5.2 Data Analysis and Results

There have been made measurements for Xe^{54+} at 5.5 MeV/u, 6 MeV/u, 6.7 MeV/u, 7 MeV/u, 8 MeV/u, 15 MeV/u and at 30.93 MeV/u with the hydrogen gas beam being switched on, and being switched off to collect information about the background radiation. The data for each energy was measured in multiple runs and written into data files, which then contained the following information: the status if the gas beam was 'on' or 'off', the photon energy measured by each of the three detectors and the time information, which will not be of interest for the further analysis. The photon energies are sorted with respect to their frequency. This allows to create a histogram, containing these data and to illustrate the photon spectrum of the Xe^{54+} ion passage through the molecular hydrogen gas target. This has been done for each energy and for the case where the gas target is 'on' and the case where it is 'off', which will in further progress of this study be referred to as T1 and T2. Then for each energy and each detector a scaling factor F is determined individually, that allows to remove the background from T1. When subtracting the measured background of T2 with this scaling factor F from the photon spectrum T1, the resulting spectra look similar to the spectrum obtained at the beam energy of 30.93 MeV/u, that can be seen in figure 19.

As can be seen in figure 19 the collected photons are measured with high intensities at certain energies, allowing to deduce the emission process during which they were emitted. The positions of the intensity peaks, and therewith the measured spectra are all characteristic for the used projectile and target material at the respective energy. Comparing the photon spectra with the spectra calculated with the programme RECAL, as described in [78, 79], allows the identification of the various peaks in figure 19. The intensities designated to K-, L-, M-, or N-REC are from photons produced during the radiative electron

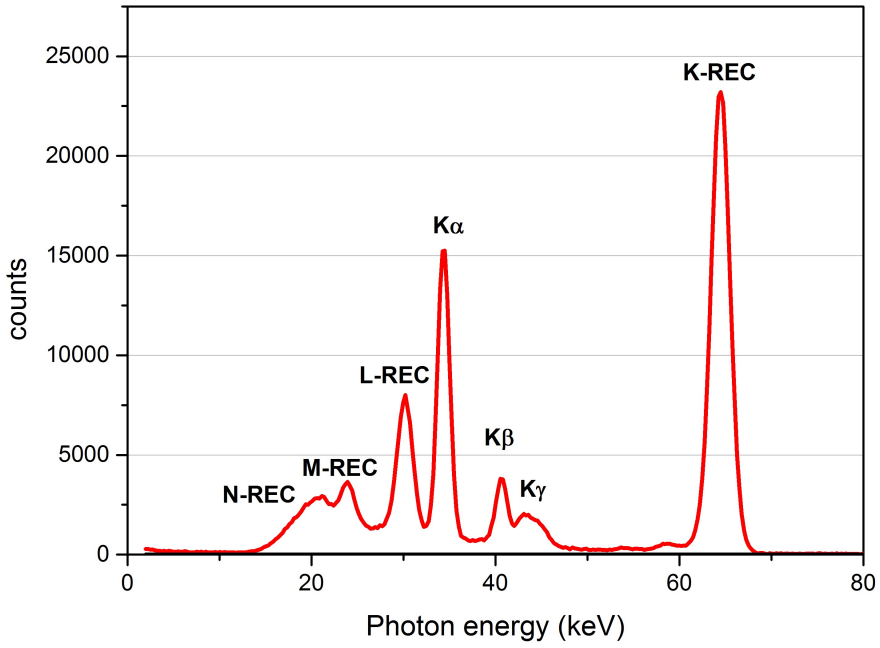

Fig. 19: Photon spectrum of Xe^{54+} projectiles colliding at 30.93 MeV/u with H_2, measured with the photon detector at 60°.

capture into the respective projectile shells. The letters K_α, K_β and K_γ denote the photons, which are emitted when an electron is transitioning from a higher shell, in this case the L-, M-, or N-shell, respectively, into the K-shell. This happens after electrons are captured either by radiative electron capture or by non-radiative electron capture into a higher atomic projectile shell. Comparing the two spectra in figure 19 and figure 20 reflects how at higher energy (see figure 19) the REC process is dominating: the intensity of K-REC is bigger than of K_α, K_β and K_γ combined, while at lower energy (see figure 20) the NRC becomes more important as it is the other way around. It can also be seen, that at the left side of the K_α in figure 20, no photon peaks were measured. This indicates, that the trigger threshold was set too high for the corresponding experiment run, to measure photons with lower energy. It should be mentioned, that even if the background, measured when the gas jet was switched off, was removed with a scaling factor as described, there was still background left. This became evident in the energy areas in between the characteristic intensity peaks, where photons from the collisions between the Xe^{54+} ions and the hydrogen atoms should not appear in the respective characteristic spectra. Therefore, each intensity was reduced by the background on its left end, when

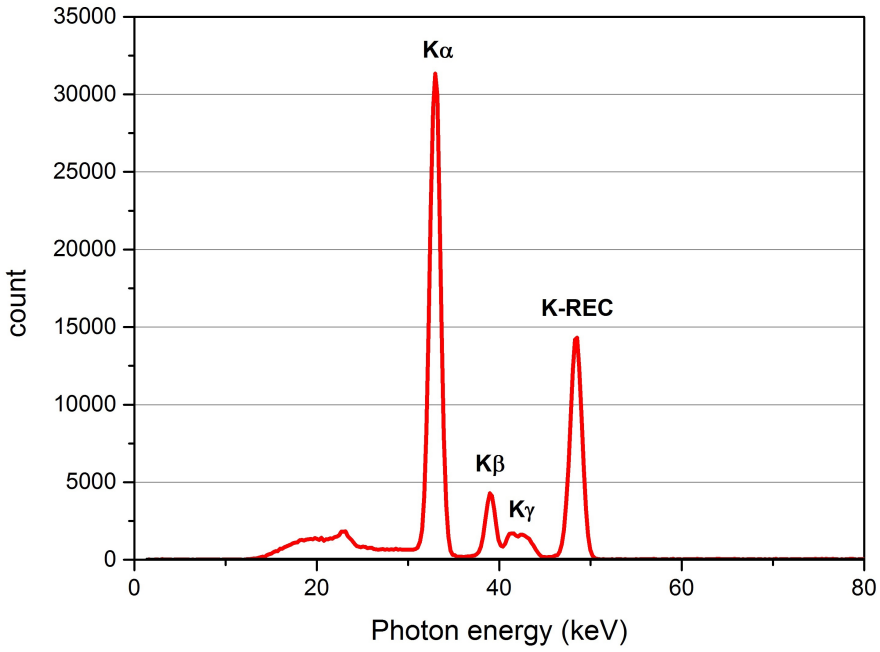

Fig. 20: Photon spectrum of Xe^{54+} projectiles colliding at 8 MeV/u with H_2, resulting from the mean value of the data measured with the photon detectors at 35° and at 60°.

used for calculations. It should also be noted, that the photons stemming from the radiative electron capture into all higher shells than the N-shell are forming the tail on the left side of the N-REC peak. The same applies for the relaxation photons resulting from electrons transitioning from shells higher than the N-shell into the K-shell, which are forming the tail on the right side of K_γ. In the following calculations K_β is denoting all photons emitted from electrons transitioning from shells higher than the L-shell, summarizing K_β, K_γ, etc. .

The electron capture cross section into the excited shells of the projectile is obtained from the emission cross section of characteristic photons (i.e. K_α and K_β) stemming from transitions into the ground state. The cross sections σ_{K_α} and σ_{K_β}, describing the emission of K-radiation, are then calculated similar to the method described in [35], by the following calculations:

$$d\sigma_{K_\alpha} = \frac{I_{K_\alpha}}{I_{\text{K-REC}}} \frac{\varepsilon_{\text{K-REC}}}{\varepsilon_{K_\alpha}} \frac{d\sigma_{\text{K-REC}}}{d\Omega} d\Omega \quad , \quad d\sigma_{K_\beta} = \frac{I_{K_\beta}}{I_{\text{K-REC}}} \frac{\varepsilon_{\text{K-REC}}}{\varepsilon_{K_\beta}} \frac{d\sigma_{\text{K-REC}}}{d\Omega} d\Omega \qquad (14)$$

where the K-radiation intensities I_{K_α}, I_{K_β}, and the REC-peak-intensity $I_{\text{K-REC}}$ are taken from the experimental spectra, the detector efficiencies at the respective peak positions are described by ε_{K_α}, ε_{K_β}, and $\varepsilon_{\text{K-REC}}$, and are determined by [80]. The differential cross section $\frac{d\sigma_{\text{K-REC}}}{d\Omega}$ is taken from the programme RECAL. Adding up the two emission cross sections σ_{K_α} and σ_{K_β} results approximately in the cross section of the electron capture process into the projectile shells of $n \geqslant 2$, measured with a detector positioned at a respective angular direction. These emission cross sections were transformed from the laboratory system into the emitter system to enable comparability of the different detector positions. Assuming that in the emitter system the emission pattern of K-radiation is isotropic allows to determine the electron capture cross section into excited states of Xe^{54+} as follows:

$$\sigma_{capture,n\geqslant 2} = \int \frac{(d\sigma_{K_\alpha} + d\sigma_{K_\beta})}{d\Omega} d\Omega = (\sigma_{K_\alpha} + \sigma_{K_\beta}) * 4\pi. \tag{15}$$

The resulting capture cross sections into the excited states are tabulated in table 5 and can be seen in figure 21, where the experimental data (black dots) is compared to the theoretical total electron capture cross sections into the excited states $n \geqslant 2$ (black line) that are the results of the NRC cross sections (blue line), calculated by the EIKONAL code, summed up with the REC cross sections (red line). These REC cross sections were calculated with the tabulated exact values presented by Ichihara et al. [29]. Since these tabulated exact values

Table 5: Electron capture cross sections into excited states of the xenon projectile in barn for the used detectors and for each energy. A cross marks when the measured data was used for the analysis. When multiple measurement results were used, a mean value was taken.

Detector at	**35°**	**60°**
5.5 MeV/u	⊗ 15028.13 b	⊗ 15386.72 b
6 MeV/u	◯ -	⊗ 11348.07 b
6.7 MeV/u	⊗ 7089.11 b	⊗ 7368.85 b
7 MeV/u	◯ -	⊗ 5840.68 b
8 MeV/u	⊗ 3576.26 b	⊗ 3765.08 b
15 MeV/u	◯ -	⊗ 710.97 b
30.93 MeV/u	◯ -	⊗ 176.71 b

are only covering the electron capture up to the M-shell, an approximation code including the formulas presented in [24] and based on [81] was used to estimate the radiative capture cross section for higher states (calculated for one hundred states for this work). The very accurate theories to determine the REC cross section and its low importance at lower energies allow to draw a conclusion about the accuracy of the used NRC cross section theory. As can be seen, the theoretical results calculated with the EIKONAL code are matching the experimental analysis results with good agreement.

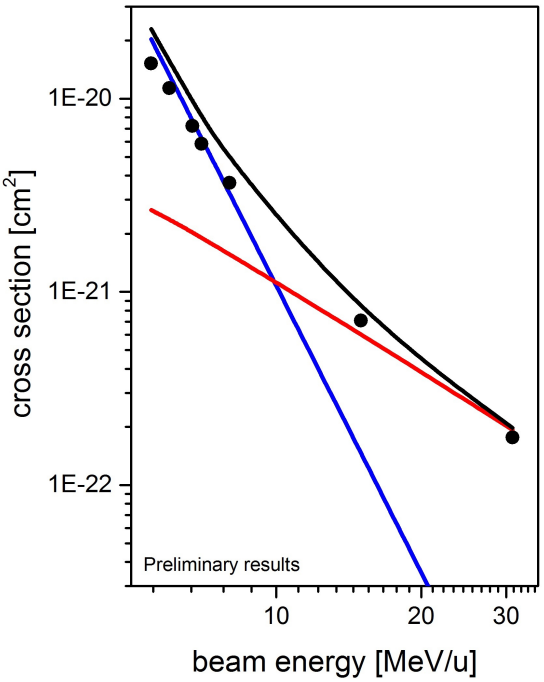

Fig. 21: Electron capture cross sections into the excited states $n \geqslant 2$ against the beam energy in MeV/u. Shown are the NRC cross sections (blue line), the REC cross sections (red line) and the resulting total capture cross sections (black line), which are compared to the experimental data (black dots).

Comparing another theory, used in the CAPTURE code of V. P. Shevelko, to the EIKONAL theory and also to the experimental data, gives the results illustrated in figure 22. Shown are again the experimental data (black dots), the total capture cross sections into the excited states $n \geqslant 2$ calculated with the REC from the tabulated values presented by Ichihara et al. with the mentioned extension, and the NRC cross sections calculated with the EIKONAL code (red

line), and with the CAPTURE code of V. P. Shevelko (green line).

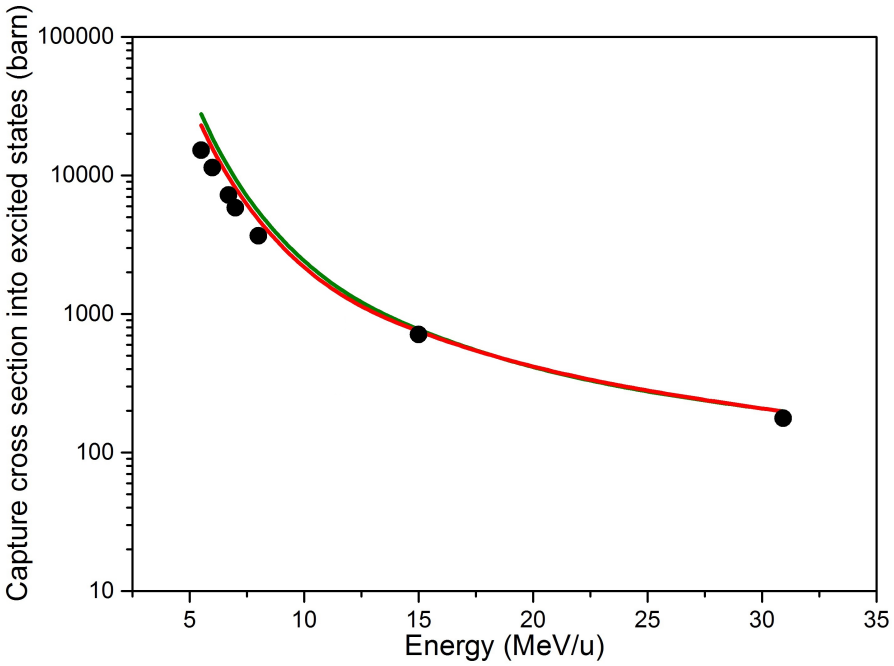

Fig. 22: The theoretical total electron capture cross sections into the excited states $n \geqslant 2$ against the beam energy (collision energy) in MeV/u, resulting as the sum of the described REC cross sections and the NRC cross sections of the CAPTURE code (green line), and of the EIKONAL code (red line). The theoretical cross sections are compared to the experimental total capture cross sections into excited states (black dots).

Another approach used to calculate the NRC cross sections in the low energy regime is the empirical Schlachter formula [82]. This formula was developed to make predictions of the total capture cross sections. Therefore the theoretical capture cross sections into the K-shell are added onto the experimental data as well as on the EIKONAL results in order to compare the resulting total capture cross sections with each other. The comparison of the Schlachter theory to the EIKONAL theory and also to the experimental data, can be seen in figure 23. The Schlachter formula can be used for systems in the reduced energy range $10 < \tilde{E} < 1000$, with $\tilde{E} = \frac{E_{kin}[keV]}{Z_T^{1.25} q^{0.7}}$, where Z_T is the target nuclear charge number and q the projectile charge. For this study the corresponding validity is going up to $\tilde{E} = 1000 \Rightarrow E_{kin} = 16\,MeV/u$.

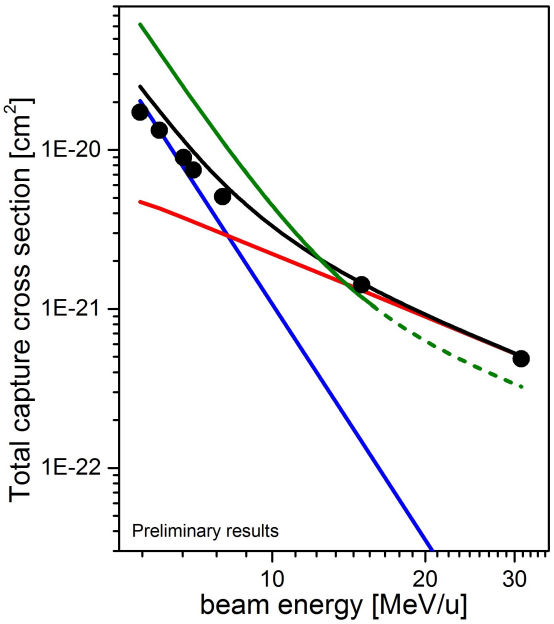

Fig. 23: The theoretical total electron capture cross sections into the excited states $n \geqslant 2$ against the beam energy (collision energy) in MeV/u, resulting as the sum of the described REC cross sections and the NRC cross sections of the Schlachter formula (green line), and of the EIKONAL code (red line). The theoretical cross sections are compared to the experimental total capture cross sections into excited states (black dots). The validity of the Schlachter formula for this projectile/target combination is going up to $E_{kin} = 16MeV/u$. A dashed line is used for beam energies that lie beyond this range.

As can be seen, the results of the Schlachter formula within the validity range are showing the same behaviour as the experimental data, but the Schlachter formula does not provide the same agreement as the EIKONAL code does. The CAPTURE code in figure 22 is also very close to the experimental data and only slightly off from the results of the EIKONAL code. The good overlap with the experimental data verifies, that the most accurate predictions of the NRC cross sections were done by the EIKONAL code, making it a suitable application for the experiments at CRYRING@GSI. This finding can be attributed to the large asymmetry between the nucleus and target charge of the collision system which favours the application of perturbation theories. Note, a similar finding can be stated for U^{92+} on N_2 collisions.

6 Summary and Conclusion

This work was motivated by the interest in partially stripped ions for experiments at upcoming heavy ion facilities, i.e. FAIR at GSI and Gamma Factory at CERN. A package of programmes and theories was compiled, which allows to predict the charge state distributions of ion beams colliding with a stripper target in order to produce efficient stripper foils. For low energies the GLOBAL code can be used, but its limit of 2000 MeV/u renders it unusable for parts of this work as ion energies may reach up to 5900 MeV/u. The recently developed BREIT code however, allows to overcome this limit, but in order to do so it needs various cross sections for the charge exchange processes, which the user needs to provide.
The BREIT code has been combined with well-tested codes for the calculation of the cross sections and then executed for an exemplary task for the upcoming GSI/FAIR facility, showing its practicability and performance. In this study a many-electron uranium projectile collided at an energy of 2700 MeV/u with different target materials going from $^{12}_{6}$C up to $^{207}_{82}$Pb in terms of the nuclear charge number. The results allowed to study the influence of the target material as well as of the target thickness on the evolution of the projectile charge state distribution. In addition also the energy loss was discussed. For low energies it is an important factor that has to be taken into account to find a suitable stripper foil for an accelerator facility. As was shown for the mentioned high relativistic energies however, the energy loss is marginal.
The full potential of the BREIT code in combination with the used cross section programmes was applied for the study for the concerning Gamma Factory at CERN. For this study calculations were done taking into account twenty-eight projectile electrons in order to find stripper foils that are able to produce efficiently Pb^{80+}, or respectively Pb^{81+} from a Pb^{54+} ion beam. The final decision about the choice of the stripper foil will have to be made after multiple experimental tests. However, the results of this work allowed to narrow down the choice of materials and thickness, where to set the starting point of the experimental tests. The possible stripper positions within the accelerator facility of CERN upstream the LHC allow the stripping energies 72.2 MeV/u and 5900 MeV/u. For the lower energy scenario the GLOBAL code was used. The calculations showed, that $^{12}_{6}$C and $^{27}_{13}$Al are providing the best yield of Pb^{80+} compared to $^{48}_{22}$Ti and $^{64}_{29}$Cu. While $^{12}_{6}$C is giving a slightly

better yield, $^{27}_{13}$Al has the advantage to induce a smaller energy loss. They also showed that producing Pb^{81+} is inefficient at this energy in general, at least for solid state stripper foils. For the scenario of 5900 MeV/u, according to the BREIT code together with the cross section programmes, the yield of both charge states is acceptable for the stripper materials $^{27}_{13}$Al, $^{48}_{22}$Ti, and $^{64}_{29}$Cu. Another result is that the $^{184}_{74}$W has to be dismissed as stripper material, due to its instability at the necessary thickness to produce the respective charge states. During the discussion turned out, that for the choice of an optimal stripper foil, aside of the yield and energy loss, also other parameters have to be taken into consideration. Therefore this work does not provide an absolute statement which stripper foil has to be used, but it acts as a guideline for the target material and thickness, that will be tested. As a result of this work $^{27}_{13}$Al and $^{48}_{22}$Ti stripper foils will be tested at CERN. They will be installed in between the PS and SPS accelerators, where the ions will be stripped at 5900 MeV/u. The experimental tests are scheduled for 2018 at CERN.

In the last chapter, data of a beam time at ESR at GSI in 2016 has been analysed and it was found, that the EIKONAL code gives a good agreement with the results for the NRC cross sections in the range of 5.5 MeV/u to 30.93 MeV/u. This verifies, that for low-Z targets but medium- to high-Z projectiles, the eikonal approximation (perturbation theory) can be applied at relatively low beam energies. This appears to be in contrast to the empirical Schlachter formula where very asymmetric collision pairs, involving bare, medium-, or high-Z ions, have not been considered. In terms of accuracy, the EIKONAL code has a big advantage over the Schlachter formula and it is slightly better than the CAPTURE code, which both were also compared to the experimental data. Finally, it was shown that the EIKONAL code is suitable to predict the NRC cross sections for the upcoming experiments at CRYRING@GSI for light targets and high-Z ions and not too low beam energies of a few MeV/u.

[1] FAIR homepage, URL: http://www.fair-center.eu/, 2017. (from 07.11.2017).

[2] T. Gaßner. *High Precision X-ray Spectroscopy of Highly Charged Heavy Ions*. PhD thesis, Friedrich-Schiller-Universität Jena, 2016.

[3] K. Blasche and D. Bohne. Status report on the GSI synchrotron facility and first beam results. In *Particle Accelerator Conference, 1989. Accelerator Science and Technology., Proceedings of the 1989 IEEE*, pages 27–28. IEEE, 1989.

[4] P. Marin and P. Mandrillon. *EPAC 90: 2nd European Particle Accelerator Conference: Nice, June 12-16, 1990*, volume 1. Atlantica Séguier Frontières, 1990.

[5] C. Omet, P. Spiller, J. Stadlmann, and D. H. H. Hoffmann. Charge change-induced beam losses under dynamic vacuum conditions in ring accelerators. *New Journal of Physics*, 8(11):284, 2006.

[6] H. H. Gutbrod, I. Augustin, H. Eickhoff, K. D. Groß, W. F. Henning, D. Krämer, and G. Walter. FAIR-baseline technical report. Executive summary. 2006.

[7] A. Dolinskii, K. Knie, C. Dimopoulou, V. Gostishchev, S. Litvinov, F. Nolden, and M. Steck. Antiproton complex at the FAIR project. *Nuclear Instruments and Methods in Physics Research Section A: Accelerators, Spectrometers, Detectors and Associated Equipment*, 629(1):16–24, 2011.

[8] T. Stöhlker, V. Bagnoud, K. Blaum, A. Blazevic, A. Bräuning-Demian, M. Durante, F. Herfurth, M. Lestinsky, Y. Litvinov, S. Neff, et al. APPA at FAIR: From fundamental to applied research. *Nuclear Instruments and Methods in Physics Research Section B: Beam Interactions with Materials and Atoms*, 365:680–685, 2015.

[9] Cern homepage. URL: http://home.cern/, 2018. (from 24.01.18).

[10] LHC Guide, URL: http://cds.cern.ch/record/2255762, 2017. (from 08.02.2018).

[11] P. Foka and M. A. Janik. An overview of experimental results from ultra-relativistic heavy-ion collisions at the CERN LHC: bulk properties and dynamical evolution. *Reviews in Physics*, 1:154–171, 2016.

[12] M. Georges. TE-EPC-LPC in LHC. URL: http://te-epc-lpc.web.cern.ch/te-epc-lpc/machines/lhc/general.stm, 2017. (from 24.01.18).

[13] M. W. Krasny. The Gamma Factory proposal for CERN. *arXiv preprint arXiv:1511.07794*, 2015.

[14] W. Barth, G. Clemente, L. Dahl, P. Gerhard, L. Groening, B. Lommel, M. S. Kaiser, M. Maier, S. Mickat, W. Vinzenz, et al. High current U40+ operation in the GSI UNILAC. *LINAC2010, MOP044*, page 154, 2010.

[15] W. R. Leo. *Techniques for Nuclear and Particle Physics Experiments, 2. Edition*. Springer-Verlag, 1994.

[16] J. C. Slater. Atomic shielding constants. *Physical Review*, 36(1):57, 1930.

[17] A. Ichihara, T. Shirai, and J. K. M. Eichler. Radiative electron capture in relativistic atomic collisions. *Physical Review A*, 49(3):1875, 1994.

[18] M. Stobbe. Zur Quantenmechanik photoelektrischer Prozesse. *Annalen der Physik*, 399(6):661–715, 1930.

[19] J. R. Oppenheimer. On the quantum theory of the capture of electrons. *Physical Review*, 31(3):349, 1928.

[20] H. A. Bethe and E. E. Salpeter. *Quantum mechanics of one- and two-electron atoms*. Plenum Press, 1997.

[21] T. Stöhlker, C. Kozhuharov, P. H. Mokler, A. Warczak, F. Bosch, H. Geissel, R. Moshammer, C. Scheidenberger, J. K. M. Eichler, A. Ichihara, et al. Radiative electron capture studied in relativistic heavy-ion-atom collisions. *Physical Review A*, 51(3):2098, 1995.

[22] G. Raisbeck and F. Yiou. Electron capture by 40-, 155-, and 600-MeV protons in thin foils of Mylar, Al, Ni, and Ta. *Physical Review A*, 4(5):1858, 1971.

[23] M. Kleber and D. H. Jakubassa. Radiative electron capture in heavy-ion collisions. *Nuclear Physics A*, 252(1):152–162, 1975.

[24] J. K. M. Eichler and T. Stöhlker. Radiative electron capture in relativistic ion-atom collisions and the photoelectric effect in hydrogen-like high-Z systems. *Physics Reports*, 439(1):1–99, 2007.

[25] G. Weber. *Untersuchung zur Anisotropie und linearen Polarisation radiativer Prozesse in energiereichen Ion-Atom-Stößen*. PhD thesis, 2010.

[26] H. W. Schnopper, H.-D. Betz, J. P. Delvaille, K. Kalata, A. R. Sohval, K. W. Jones, and H. E. Wegner. Evidence for radiative electron capture by fast, highly stripped heavy ions. *Physical Review Letters*, 29(14):898, 1972.

[27] P. Kienle, M. Kleber, B. Povh, R. M. Diamond, F. S. Stephens, E. Grosse, M. R. Maier, and D. Proetel. Radiative capture and bremsstrahlung of bound electrons induced by heavy ions. *Physical Review Letters*, 31(18):1099, 1973.

[28] C. Scheidenberger, T. Stöhlker, W. E. Meyerhof, H. Geissel, P. H. Mokler, and B. Blank. Charge states of relativistic heavy ions in matter. *Nuclear Instruments and Methods in Physics Research Section B: Beam Interactions with Materials and Atoms*, 142(4):441–462, 1998.

[29] A. Ichihara and J. K. M. Eichler. Cross sections for radiative recombination and the photoelectric effect in the K, L, and M shells of one-electron systems with $1 \leq Z \leq 112$ calculated within an exact relativistic description. *Atomic Data and Nuclear Data Tables*, 74(1):1–121, 2000.

[30] J. K. M. Eichler. Relativistic eikonal theory of electron capture. *Physical Review A*, 32(1):112, 1985.

[31] J. K. M. Eichler. Eikonal theory of charge exchange between arbitrary hydrogenic states of target and projectile. *Physical Review A*, 23(2):498, 1981.

[32] J. K. M. Eichler and H. Narumi. On the classical-trajectory eikonal approximation for electron capture into multicharged ions. *Zeitschrift für Physik A Hadrons and Nuclei*, 295(3):209–214, 1980.

[33] L. J. Dubé and J. K. M. Eichler. Structural and asymptotic properties of the eikonal approximation for electron capture. *Journal of Physics B: Atomic and Molecular Physics*, 18(12):2467, 1985.

[34] W. E. Meyerhof, R. Anholt, J. K. M. Eichler, H. Gould, C. Munger, J. Alonso, P. Thieberger, and H. E. Wegner. Atomic collisions with relativistic heavy ions. III. Electron capture. *Physical Review A*, 32(6):3291, 1985.

[35] T. Stöhlker, T. Ludziejewski, H. Reich, F. Bosch, R. W. Dunford, J. K. M. Eichler, B. Franzke, C. Kozhuharov, G. Menzel, P. H. Mokler, et al. Charge-exchange cross sections and beam lifetimes for stored and decelerated bare uranium ions. *Physical Review A*, 58(3):2043, 1998.

[36] H. F. Krause, C. R. Vane, S. Datz, P. Grafström, H. Knudsen, U. Mikkelsen, C. Scheidenberger, R. H. Schuch, and Z. Vilakazi. Electron capture and ionization of 33-TeV Pb ions in gas targets. *Physical Review A*, 63(3):032711, 2001.

[37] P. A. M. Dirac. A theory of electrons and protons. In *Proc. R. Soc. Lond. A*, volume 126, pages 360–365. The Royal Society, 1930.

[38] P. Grafström, S. Datz, H. F. Krause, C. R. Vane, H. Knudsen, U. Mikkelsen, R. H. Schuch, C. Scheidenberger, and Z. Vilakazi. Measurement of electromagnetic cross sections in heavy ion interactions and its consequences for luminosity lifetimes in ion colliders. *Particle Accelerator Conference, 1999. Proceedings of the 1999*, 3:1671–1673, 1999.

[39] C. R. Vane, S. Datz, P. F. Dittner, H. F. Krause, R. Schuch, H. Gao, and R. Hutton. Knock-on electrons produced in collisions of 6.4 TeV sulfur ions with fixed targets. *Nuclear Instruments and Methods in Physics Research Section B: Beam Interactions with Materials and Atoms*, 79(1-4):26–29, 1993.

[40] C. R. Vane, S. Datz, H. F. Krause, P. F. Dittner, E. F. Deveney, H. Knudsen, P. Grafström, R. Schuch, H. Gao, and R. Hutton. Atomic collisions with 33-TeV lead ions. *Physica Scripta*, 1997(T73):167, 1997.

[41] H. F. Krause, C. R. Vane, S. Datz, P. Grafström, H. Knudsen, C. Scheidenberger, and R. H. Schuch. Electron capture and ionization of Pb ions at 33 TeV. *Physical Review Letters*, 80(6):1190, 1998.

[42] C. R. Vane, H. F. Krause, S. Datz, P. Grafström, H. Knudsen, C. Scheidenberger, and R. H. Schuch. Radiative electron capture at ultrarelativistic energies: 33-TeV Pb 82+ ions. *Physical Review A*, 62(1):010701, 2000.

[43] I. Y. Tolstikhina and V. P. Shevelko. Collision processes involving heavy many-electron ions interacting with neutral atoms. *Physics-Uspekhi*, 56(3):213, 2013.

[44] I. Y. Tolstikhina, I. I. Tupitsyn, S. N. Andreev, and V. P. Shevelko. Influence of relativistic effects on electron-loss cross sections of heavy and superheavy ions colliding with neutral atoms. *Journal of Experimental and Theoretical Physics*, 119(1):1–7, 2014.

[45] I. Y. Tolstikhina and V. P. Shevelko. Electron-capture cross sections in collisions of multielectron ions with atoms. CAPTURE code. *Short Commun*, 5:40–48, 2000.

[46] V. P. Shevelko, I. Y. Tolstikhina, and T. Stöhlker. Stripping of fast heavy low-charged ions in gaseous targets. *Nuclear Instruments and Methods in Physics Research Section B: Beam Interactions with Materials and Atoms*, 184(3):295–308, 2001.

[47] I. L. Beigman, I. Y. Tolstikhina, and V. P. Shevelko. Ionization of heavy ions in relativistic collisions with neutral atoms. *Technical Physics*, 53(5):547–553, 2008.

[48] V. P. Shevelko, I. L. Beigman, M. S. Litsarev, H. Tawara, I. Y. Tolstikhina, and G. Weber. Charge-changing processes in collisions of heavy many-electron ions with neutral atoms. *Nuclear Instruments and Methods in Physics Research Section B: Beam Interactions with Materials and Atoms*, 269(12):1455–1463, 2011.

[49] G. Baur, I. L. Beigman, V. P. Shevelko, I. Yu. Tolstikhina, and T. Stöhlker. Ionization of highly charged relativistic ions by neutral atoms and ions. *Physical Review A*, 80:012713, Jul 2009.

[50] J. Eichler and W. E. Meyerhof. *Relativistic Atomic Collisions*. Academic Press, San Diego, 1995.

[51] A. N. Artemyev, V. M. Shabaev, T. Stöhlker, and A. S. Surzhykov. Negative-continuum dielectronic recombination into excited states of highly charged ions. *Physical Review A*, 79(3):032713, 2009.

[52] A. Voitkiv and J. Ullrich. *Relativistic Collisions of Structured Atomic Particles*, volume 49. Springer Science & Business Media, 2008.

[53] R. Moshammer, W. Schmitt, J. Ullrich, H. Kollmus, A. Cassimi, R. Dörner, O. Jagutzki, R. Mann, R. E. Olson, H. T. Prinz, et al. Ionization of helium in

the attosecond equivalent light pulse of 1 GeV/nucleon U92+ projectiles. *Physical Review Letters*, 79(19):3621, 1997.

[54] A. Voitkiv. Theory of projectile-electron excitation and loss in relativistic collisions with atoms. *Physics reports*, 392(4):191–277, 2004.

[55] T. Stöhlker, H. Backe, H. F. Beyer, F. Bosch, A. Bräuning-Demian, S. Hagmann, D. C. Ionescu, K. Jungmann, H.-J. Kluge, C. Kozhuharov, et al. Status and perspectives of atomic physics research at GSI: The new GSI accelerator project. *Nuclear Instruments and Methods in Physics Research Section B: Beam Interactions with Materials and Atoms*, 205:156–161, 2003.

[56] J. D. Jackson. *Classical electrodynamics*. American Association of Physics Teachers, 1999.

[57] T. Stöhlker, R. Schuch, S. Hagmann, Y. A. Litvinov, C. Dimopoulou, A. Dolinskii, and M. Steck. SPARC experiments at the HESR: a feasibility study. *GSI Scientific Report*, volume 477, 2011.

[58] R. P. Feynman, R. B. Leighton, and M. Sands. The Feynman lectures on physics. *Quantum Mechanics*, 2:1, 1965.

[59] URL: http://physik.wikia.com/wiki/Detektoren, 2018. (from 11.02.2018).

[60] W. R. Leo. *Techniques for nuclear and particle physics experiments: a how-to approach*. Springer, 1987.

[61] URL: http://web-docs.gsi.de/ aprochaz/webatima/, 2017. (from 02.11.2017).

[62] J. Lindhard, A. H. Sørensen, et al. Relativistic theory of stopping for heavy ions. *Physical Review A*, 53(4):2443, 1996.

[63] S. Datz, H. F. Krause, C. R. Vane, H. Knudsen, P. Grafström, and R. H. Schuch. *Physical Review Letters*, 77(14):2925, 1996.

[64] N. Winckler, A. Rybalchenko, V. P. Shevelko, M. Al-Turany, T. Kollegger, and T. Stöhlker. BREIT code: Analytical solution of the balance rate equations for charge-state evolutions of heavy-ion beams in matter. *Nuclear Instruments and Methods in Physics Research Section B: Beam Interactions with Materials and Atoms*, 392:67–73, 2017.

[65] G. Schiwietz and P. L. Grande. Improved charge-state formulas. *Nuclear Instruments and Methods in Physics Research Section B: Beam Interactions with Materials and Atoms*, 175:125–131, 2001.

[66] H.-D. Betz. Charge states and charge-changing cross sections of fast heavy ions penetrating through gaseous and solid media. *Reviews of Modern Physics*, 44(3):465, 1972.

[67] H. Weick. URL: https://web-docs.gsi.de/∼weick/charge_states/, 2017. (from 22.11.2017).

[68] LISE++ homepage, URL: http://lise.nscl.msu.edu/, 2017. (from 22.11.2017).

[69] GitHub/FAIR-BREIT homepage, URL: https://github.com/FAIR-BREIT/, 2017. (from 22.11.2017).

[70] N. Winckler, A. Rybalchenko, V. P. Shevelko, M. Al-Turany, T. Kollegger, and T. Stöhlker. URL: http://breit.gsi.de/, 2017. (from 22.11.2017).

[71] S. K. Allison. Experimental results on charge-changing collisions of hydrogen and helium atoms and ions at kinetic energies above 0.2 keV. *Reviews of Modern Physics*, 30(4):1137, 1958.

[72] R. Anholt. Calculation of *K*-vacancy production by relativistic projectiles. *Physical Review A*, 19:1004–1010, Mar 1979.

[73] N. Claytor, A. Belkacem, T. Dinneen, B. Feinberg, and Harvey Gould. Ionization of Au^{78+} and electron capture by Au^{79+} at 10.8 GeV/nucleon. *Physical Review A*, 55:R842–R845, Feb 1997.

[74] T. A. Carlson, C. W. Nestor, N. Wasserman, and J. D. McDowell. Calculated ionization potentials for multiply charged ions. *Atomic Data and Nuclear Data Tables*, 2:63–99, 1970.

[75] P. Rymuza, T. Stöhlker, C. L. Cocke, H. Geissel, C. Kozhuharov, P. H. Mokler, R. Moshammer, F. Nickel, C. Scheidenberger, Z. Stachura, et al. Deviation from first-order perturbation theory observed at intermediate relativistic velocities for the ionisation of highly-charged heavy projectiles. *Journal of Physics B: Atomic, Molecular and Optical Physics*, 26(7):L169, 1993.

[76] G. Strang. *Introduction to linear algebra*. 3rd ed., Wellesley-Cambridge Press, 1998.

[77] Private communication T. Stoehlker, 2017.

[78] G. Weber, H. Ding, M. O. Herdrich, and A. Surzhykov. Towards a fast calculator for the radiation characteristics of radiative recombination and radiative electron capture. 599(1):012040, 2015.

[79] M.O. Herdrich, G. Weber, A. Gumberidze, Z.W. Wu, and T. Stöhlker. Fast calculator for X-ray emission due to radiative recombination and radiative electron capture in relativistic heavy-ion atom collisions. *Nuclear Instruments and Methods in Physics Research Section B: Beam Interactions with Materials and Atoms*, 408(Supplement C):294–300, 2017. Proceedings of the 18th International Conference on the Physics of Highly Charged Ions (HCI-2016), Kielce, Poland, 11-16 September 2016.

[80] Private communication M. O. Herdrich, 2017.

[81] A. Burgess, Mem. R. Astron. Soc., 69:1, 1964.

[82] A. S. Schlachter, J. W. Stearns, W. G. Graham, K. H. Berkner, R. V. Pyle, and J. A. Tanis. Electron capture for fast highly charged ions in gas targets: An empirical scaling rule. *Physical Review A*, 27(6):3372, 1983.

Acknowledgement

I would like to express my sincere gratitude to everyone who was involved in the process of my master's thesis. Special thanks to:

- Prof. Dr. Thomas Stöhlker for giving me the opportunity to do this work at the Institute of Optics and Quantum Electronics Jena in collaboration with the Helmholtz Institute Jena, and for allowing me to participate in so many interesting projects. His guidance and continuous support helped me through my research and writing of this thesis.
- Dr. Günter Weber whose door was always open whenever I had a question about my research or writing. He consistently allowed me to overcome problems by steering me in the right direction whenever I needed it.
- Dr. Viatcheslav Shevelko for supporting me with calculation data crucial for the progress of my charge state distribution studies.
- the Gamma Factory CERN study group for the possibility to participate in such an interesting project.
- Dr. Jan Glorius for providing me with experimental data, that allowed me to realise my electron capture cross section analysis study.
- M.Sc. Oliver Herdrich and M.Sc. Marco Vockert who supported me with some calculation programmes during my studies.

Finally, I would like to express my very profound gratitude to my girlfriend Laurence Frank, my sister Svenja Kröger and my brother Florian Kröger, as well as my parents Monika Boguschewski and Detlef Kröger for the mental support and their patience during the course of my studies in the last years.

Statutory Declaration

I herewith declare that I have composed the present thesis myself and without use of any other than the cited sources and aids. Sentences or parts of sentences quoted literally are marked as such; other references with regard to the statement and scope are indicated by full details of the publications concerned. The thesis in the same or similar form has not been submitted to any examination body and has not been published. This thesis was not yet, even in part, used in another examination or as a course performance.

Place, Date	Felix Kröger